



## Dynamic analysis of flexible-link manipulator in underwater applications using Gibbs-Appell formulations

S.F. Dehkordi

Noor Branch, Iran University of Science and Technology, Noor, Iran

### ARTICLE INFO

**Keywords:**

Underwater flexible manipulator  
Fluid media & flexible links manipulator interaction  
Drag & lift effects on the robot links fluctuations  
Recursive gibbs-appell formulation

### ABSTRACT

The dynamic model of a flexible robotic chain by considering its motion in a fluid medium is developed in this study. The use of flexible manipulators in fluid applications offers several advantages, but the fluid-manipulator interaction forces, as well as the elasticity of each link, complicates the modeling process. To tackle this issue, the dynamic effects of the fluid on the performance of flexible arms are identified and expressed mathematically so that the resulting interaction during the robot motion can be modeled simultaneously. In this regard, the dynamic interaction between the links and the fluid as a result of link flexibility is modeled as a distributed load along the arm length. In addition to the structural damping of the links, the effect of fluid damping along with its added mass affects the performance of the considered robotic system. Thus, compared to a flexible robotic arm in the air or a rigid robotic arm in the fluid, the flexible deformation of the robot links during motion is affected by the fluid flow. The recursive Gibbs-Apple formulation is used to derive the equations of motion of an N-link robotic chain. Not only does this formulation reduce the computational complexity compared to similar algorithms, but it also allows us to consider the effect of forces exerted on the joints and robot links in the form of the Rayleigh dissipation function. The final equations of motion are simulated using MATLAB for a two-link flexible arm. Simulations of robot links are conducted for different elasticities, different initial conditions, and different media with different viscosities. According to the obtained results, the deformation of flexible manipulators decreases from 5 mm (in the air) to 3 mm (in the fluid), while the displacement in water is 10% of that in the air under similar conditions.

### 1. Introduction

Today, the use of flexible robotic manipulators is a topic of interest in various applications due to their agility, accuracy, high speed of operation, and optimal energy consumption. The high load-to-weight ratio of flexible manipulators helps to expand their application in space exploration, manufacturing plants, industry, transportation, and domestic applications. Extensive research has been conducted in the field of design, dynamic modeling, and control of flexible manipulators (Wang and Cui, 2021). Aided by the obtained results, the complexities of modeling and controlling this type of robot due to the unwanted vibrations of flexible arms during motion are largely eliminated. Nonetheless, the conditions for dynamic analysis are not constant and the equations need to be updated when a change in the operating environment of the robotic arm occurs and other stimuli besides the torque in the motors of joints are added (Mohammed, 2018). The use of flexible robotic arms with long links is under consideration in underwater missions that humans are unable to perform. Some examples are

manipulators that are used in underwater exploration robots to move objects and troubleshoot oil and electricity transmission lines, as well as in commercial applications in deep pools (Sivc̄ev et al., 2018). In such applications, these devices are used as underwater robots, underwater manipulators, and autonomous underwater vehicle-manipulators systems (AUVMA) (Huang et al., 2017; Underwater Robots – 2nd Edition, 2006). Notwithstanding, robotic arms in these structures are often initially composed of rigid links and the effect of fluid-robot interaction is concentrated, although computing the forces resulting from the mentioned interaction is approximated as a function of the robot dimensions. As a result, the obtained equations of motion do not differ from the actual results merely due to uncertainties and external disturbances. Therefore, approximating the forces exerted by the fluid, which is a combination of fluid drag, lift, buoyancy, and gravitational forces generates a difference in the outputs of the dynamic model from the actual system behavior (Gümǖsel and Özmen, 2011). The operation type of underwater robotic systems (i.e., remotely controlling the mechatronic system) highlights the importance of deriving their motion

E-mail addresses: [S.fathollahidehkordi@gmail.com](mailto:S.fathollahidehkordi@gmail.com), [S\\_fathollahidehkordi@mecheng.iust.ac.ir](mailto:S_fathollahidehkordi@mecheng.iust.ac.ir).

<https://doi.org/10.1016/j.oceaneng.2021.110057>

Received 13 May 2021; Received in revised form 12 September 2021; Accepted 17 October 2021

Available online 28 October 2021

0029-8018/© 2021 Elsevier Ltd. All rights reserved.

equations. Nevertheless, the advantage of using such equipment is their autonomous performance. This shows the significance of providing an accurate dynamic model based on which an appropriate control algorithm can be developed (Cai et al., 2020; Lapierre et al., 2003; Lionel, 2006a, 2006b; Sharma et al., 2019; Sharma and Saha, 2021; Wang et al., 2018; Yuguang and Fan, 2019). Thus, extending the application of flexible robots within the fluid medium depends on the proper presentation of dynamic models that consider fluid robot's link interactions extensively. For this purpose, the method of modeling, the hypotheses used, and the choice of dynamic formulation for the derivation of equations because of future applications are consequential. This new application has the main difference due to the environments and the new conservative and Non-conservative forces which are made the new performance in comparison to the reviewed cases. Hence, the process algorithm to evaluate the final motion equations was incomparable.

In modeling flexible robotic chains, obtaining an exact solution is impossible due to the nonlinear robot dynamics and the number of interconnected links (Lee and Alandoli, 2020). This is exacerbated by taking the dynamic effects of fluid into account. Numerical methods are thus used to model the flexible links of robotic arms. These methods are categorized as numerical methods based on the amplitude of link deformation (Sharifnia, 2018). In small deformations, the use of the assumed modes method (AMM) based on the mode shapes of continuous beams along with the proper boundary conditions considerations and applied forces are utilized (Korayem et al., 2019). When extracting mode shapes, one of the Euler-Bernoulli, Rayleigh, Shear, and Timoshenko beam assumptions is used by researchers. Concerning large deformations in robot links, however, the use of the finite element method (FEM) is preferable (Al-khafaji Ali, 2014). Environmental impacts and structural damping are among influential parameters in vibrational behavior in modeling flexible links. As a result, one needs to consider the differences in the fluctuating behavior of the links in the air/fluid in the process of measuring vibrational modes (Liu and Liu, 2020; Qiu et al., 2019).

Another important matter in deriving underwater dynamic equations is calculating the action/reaction between nonlinear and nonconservative forces from the fluid field as influential parameters in the motion of robotic arms. In the motion equation of robotic chains, however, internal forces are neglected to reduce the computational complexity and manipulations via an appropriate derivation algorithm. One can mention different formulations for this purpose, including Newton-Euler, Lagrange, and Kane (Rong et al., 2019). Although the concluded motion equations from these techniques are similar, they differ in computational complexity and the required time to arrive at the final equations. This highlights the importance of choosing the right approach when deriving the motion equations in accordance with system complexities and environmental conditions (Korayem and Dehkordi, 2017). Using Kane's method is the optimal choice when the external forces and final terms of the motion equation can be accurately identified (Tarn et al., 1996). It means that the coefficients of motion equations are evaluated directly by considering the extraction process in this method. Regarding energy-based methods exploited in complex dynamic systems, the Gibbs-Appell formulation results in less computational complexity than Lagrange equations (Korayem and Dehkordi, 2019), although the Newton-Euler technique offers more accurate results when evaluating the internal forces of the system (Korayem et al., 2021). Obtaining experimental modeling coefficients as a result of nonlinear robot behavior in different environments makes the input-output-based identification and exploitation methods interesting subjects for expressing the dynamic behavior of flexible robots (Mat Darus and Al-Khafaji, 2021). It should be noted that improving the results requires the use of empirical data in different operation conditions in view of the wide range of experimental tests (Mohammed et al., 2019).

Computing the hydrodynamic and hydrostatic forces exerted on underwater manipulators depends on the fluid flow conditions as well as

the geometry and material/structure of robotic arms. The forces applied from the fluid can be either dependent or independent of the motion state of the manipulator. In most previous studies, these forces have simply been considered to be concentrated so that the complexity and size of calculation for obtaining the dynamic equations could be mitigated. If preliminary assumptions for deriving the equations change, then the fluid motion should also be considered. Additionally, the experimental coefficients used in such equations are generally reliant on the geometry of manipulators (Kolodziejczyk, 2018). In modeling underwater robots, obtaining accurate equations is necessary to correctly express the drag. The description of drag inside the fluid medium is achieved via nonlinear relations and as a concentrated term in the drag center. To consider the effect of this force in the elastic deformation of flexible manipulators under similar conditions, one must recalculate them as a distributed force over the length of the robotic arm (Salloom et al., 2020; Sharma et al., 2019). Especially, it was not possible to consider the effects of links and fluid medium interactions just as an external load. As a result, it should be checked by recognizing the main effects imported to the general behavior of the robot.

The present paper focuses on the extensive usage of underwater flexible robots. For this purpose, the robot's equations of motion obtained in the air are derived again after considering the hydrodynamic and hydrostatic effects of fluid-flexible arms interaction. The main novelty of this article is to present a dynamic model of underwater N-link flexible robots given the effect of hydrodynamic and hydrostatic interaction between the robot arms and the surrounding fluid medium. Given that the dynamic model of flexible robotic chains has an infinite number of degrees of freedom due to the elasticity of robot links, the impact of hydrostatic and hydrodynamic interaction is considered as a distributed load along with the link in order to accurately investigate their effect on their vibrations. Owing to the importance of dynamic stability, the time response of the robot due to the torques applied to the joints is evaluated. The results are examined and validated for different link elasticities, different initial conditions, and different fluids. In the following, in Section 2, the kinematic modeling of an underwater flexible N-link robotic chain is discussed. In Section 3, the dynamic equations are derived using the recursive Gibbs-Appell formulation. Finally, Section 4 contains some simulations in different conditions to validate the obtained equations.

## 2. Kinematic modeling of the underwater N-link flexible robotic chain

The kinematic equations of robotic arms in view of the fluid medium are derived in this section. To this end, one needs to select reference and local coordinate systems for the robotic chain, then obtain the related kinematic equations which are used to derive the dynamic equations.

### 2.1. Coordinate system attached to the flexible robotic chain

The robotic arm in question is comprised of N flexible links connected via revolute joints, with each joint being excited using the attached electric motor. Accordingly, describing its rigid-body motion requires N generalized coordinates so that the motion of the gripper of the robotic chain can be fully expressed. To define the gripper motion including its position and orientation, the forward kinematic equations are employed. Denavit-Hartenberg convention is used to name the coordinate system attached to each link (John J. Craig, 2018). Fig. 1 shows the arrangement of coordinate systems according to this scheme.

To describe the motion trajectory of the grippers of the robotic manipulator in three-dimensional space, the selected coordinate system must provide three degrees of freedom for its position and three degrees of freedom for its angular position known as Euler angles. The links in Fig. 1 are assumed to be rigid, and no independent coordinate system is defined to describe the deformation of arms. The reference frame  $X_0Y_0Z_0$  is used to designate the absolute motion of manipulators (i.e., fixed

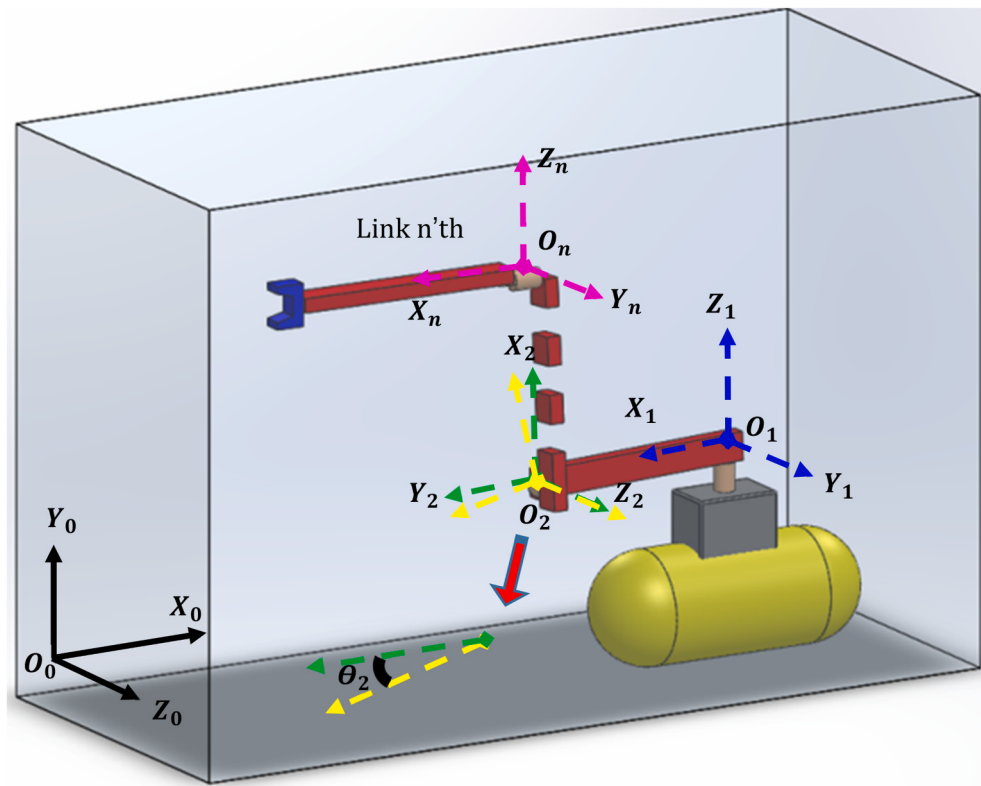


Fig. 1. Position of the coordinate system on the underwater N-link manipulator.

coordinate system). Accordingly, since the base of the robotic manipulator cannot move, the first coordinate system is placed on the manipulator's base so that the motion of the first joint of the manipulator is computed relative to this frame. To describe the motion of each of the links in the manipulator, a coordinate system is placed on the corresponding joint which defines the rotation of that specific link. Thus,  $N$  coordinate systems are necessary to express the rigid-body motion of the robotic manipulator. This choice of coordinate systems implies a generalized coordinate system of  $\theta = [\theta_1, \dots, \theta_n]^T$  for the rigid-body

motion of the  $N$ -link robotic chain, where  $\theta_i$  is the generalized coordinate of the revolute joint.

The inherent elasticity of the links in the structure of robots is their source of longitudinal, bending, and torsional vibrations. This behavior necessitates the use of a coordinate system in each link so that the elastic deformation of different links can be calculated with respect to these coordinate systems. The difference between the coordinate system attached to the link and the one attached to the joint is a measure of the rotation caused by the link flexibility and joint rotation. Fig. 2 shows the  $i$ 'th link of the  $N$ -link flexible manipulator. To describe the vibrational

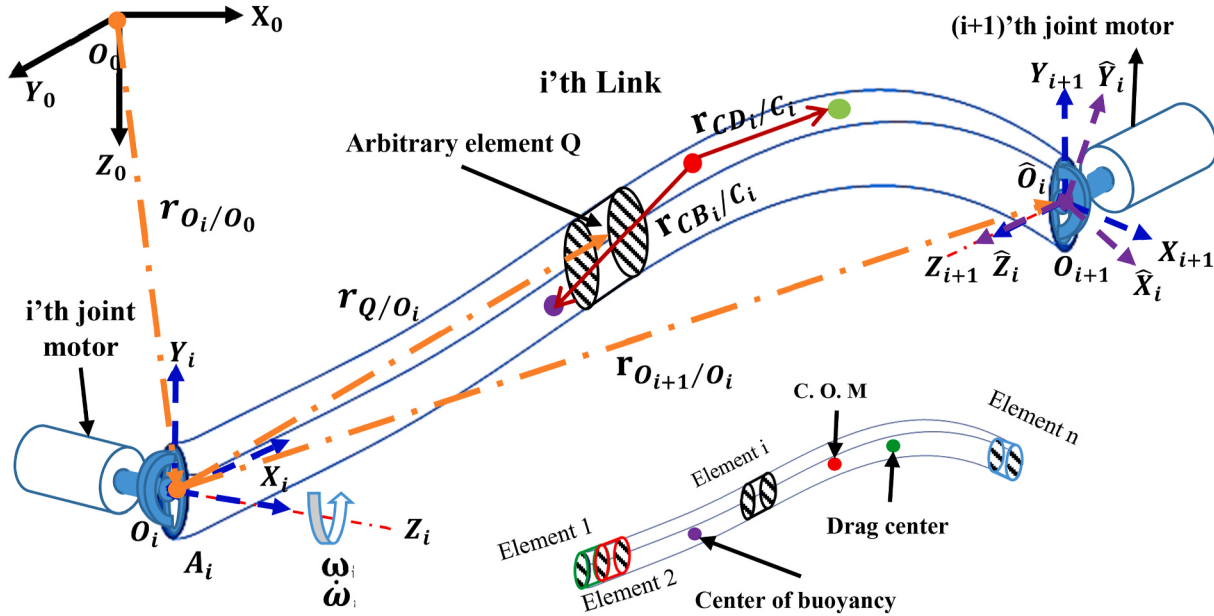


Fig. 2. Kinematics of the  $i$ 'th link of  $N$ -link flexible robotic chain.

motion of the flexible link, the coordinate system attached to the end of each link is used. Hence, the  $\hat{x}$ -axis of this coordinate system is assumed to lie along with the deformed link of the robotic chain. Also, its  $\hat{z}$ -axis aligns with the  $z$ -axis of the coordinate system on the revolute joint.

The AMM is employed to express the elastic deformation of arms. This is realized by defining the generalized modal coordinates  $\boldsymbol{\Lambda} = [\delta_{11}, \dots, \delta_{1m_1}, \dots, \delta_{n1}, \dots, \delta_{nm_n}]^T$  where  $n$  denotes the number of links,  $m$  represents the number of generalized modal coordinates of each link, and  $\delta_{ij}$  signifies the  $j$ 'th generalized modal coordinate of the  $i$ 'th link. Therefore, the number of degrees of freedom (DOFs) of the system in general equals  $N$  rigid-body DOFs of the robotic manipulator and  $mN$  DOFs associated with the elastic motion of the flexible links of the manipulator. It should be mentioned that the infinite DOFs of flexible manipulators are equal to  $mN$  DOFs by AMM (Korayem et al., 2014). Accordingly, the vector of the generalized coordinates of the  $N$ -link robotic manipulator with  $m_n$  generalized modal coordinates for each link is written as  $\boldsymbol{\Theta} = [\theta_1 \ \Lambda_1 \ \dots \ \theta_n \ \Lambda_n]^T$ . The generalized velocities of the considered robotic system are expressed as  $\dot{\boldsymbol{\Theta}} = [\dot{\theta}_1 \ \dot{\Lambda}_1 \ \dots \ \dot{\theta}_n \ \dot{\Lambda}_n]^T$ .

## 2.2. Forward kinematics of underwater flexible robotic chain

According to Fig. 2, to calculate the position vector, linear velocity, angular velocity, and vector of linear acceleration as well as the angular

to the  $i$ 'th and  $(i-1)$ 'th link and is obtained as  ${}^i\mathbf{R}_i = {}^j\mathbf{R}_{i-1}\mathbf{E}_{i-1}\mathbf{A}_i$  using recursive evaluation, the matrix  $\mathbf{A}_i$  is the rotation matrix of the  $i$ 'th joint, and  $\mathbf{E}_i$  is the rotation matrix as a result of link elasticity (Korayem and Shafei, 2013). Using Equation (2) and differentiation with respect to time, the velocity vector of the differential element  $Q$  can be found as

$${}^i\dot{\mathbf{r}}_Q = {}^i\boldsymbol{\omega}_i \times {}^i\dot{\mathbf{r}}_{Q/O_i} + {}^i\dot{\mathbf{r}}_{Q/O_i} + {}^i\ddot{\mathbf{r}}_{O_i} \quad \text{where } {}^i\dot{\mathbf{r}}_{Q/O_i} = \sum_{j=1}^{m_i} \mathbf{r}_{ij}(\eta) \dot{\delta}_{ij}(t) \quad (3)$$

where the vector  ${}^i\boldsymbol{\omega}_i$  represents the angular velocity of the  $i$ 'th link as in

$${}^i\boldsymbol{\omega}_i = {}^i\mathbf{z}_i \dot{\theta}_i + {}^i\mathbf{R}_{i-1} \left( {}^{i-1}\boldsymbol{\omega}_{i-1} + {}^{i-1}\dot{\boldsymbol{\phi}}_{i-1}(L_{i-1}) \right) \quad (4)$$

where  $\dot{\theta}_i$  is the angular velocity of the  $i$ 'th link, the angle  $\boldsymbol{\phi}$  is a function of the elastic deformation of robot links and is found using the AMM ( $\boldsymbol{\Phi}_i = \sum_{j=1}^{m_i} \boldsymbol{\Phi}_{ij}(\eta) \delta_{ij}(t)$ ). Also,  $\boldsymbol{\Phi}_{ij}$  is the vector of the mode shapes of elastic angular displacement of robot links, representing the  $j$ 'th rotational mode shape of  $i$ 'th link. In addition,  ${}^i\dot{\mathbf{r}}_{O_i}$  and  ${}^i\ddot{\mathbf{r}}_{O_i}$  are found recursively in the form

$${}^i\ddot{\mathbf{r}}_{O_i} = {}^i\mathbf{R}_{i-1} \left( \left( {}^{i-1}\dot{\boldsymbol{\omega}}_{i-1} \times {}^{i-1}\mathbf{r}_{O_i/O_{i-1}} \right) + 2 \cdot \left( {}^{i-1}\boldsymbol{\omega}_{i-1} \times {}^{i-1}\dot{\mathbf{r}}_{O_i/O_{i-1}} \right) + {}^{i-1}\boldsymbol{\omega}_{i-1} \times \left( {}^{i-1}\boldsymbol{\omega}_{i-1} \times {}^{i-1}\mathbf{r}_{O_i/O_{i-1}} \right) + {}^{i-1}\ddot{\mathbf{r}}_{O_{i-1}} \right) \quad (5)$$

acceleration of different components of the robotic system, the differential element  $Q$  is arbitrarily chosen on the  $i$ 'th link.  ${}^i\mathbf{r}_{Q/O_i}$  is the position vector of the arbitrary differential element  $Q$  in the local coordinate system. The position vector of this element relative to the local coordinate system attached to the  $i$ 'th link ( $O_i$ ) is described as

$${}^i\mathbf{r}_{Q/O_i} = \eta {}^i\mathbf{x}_i + \sum_{j=1}^{m_i} \mathbf{r}_{ij}(\eta) \delta_{ij}(t) \quad (1)$$

$${}^i\dot{\boldsymbol{\omega}}_i = {}^i\mathbf{z}_i \ddot{\theta}_i + {}^i\mathbf{R}_{i-1} \left( {}^{i-1}\dot{\boldsymbol{\omega}}_{i-1} + {}^{i-1}\ddot{\boldsymbol{\Phi}}_{i-1}(L_{i-1}) + {}^{i-1}\boldsymbol{\omega}_{i-1} \times {}^{i-1}\dot{\boldsymbol{\phi}}_{i-1}(L_{i-1}) \right) + {}^i\mathbf{R}_{i-1} \left( {}^{i-1}\boldsymbol{\omega}_{i-1} + {}^{i-1}\dot{\boldsymbol{\phi}}_{i-1}(L_{i-1}) \right) \times {}^i\mathbf{z}_i \dot{\theta}_i \quad (8)$$

where  ${}^i\mathbf{x}_i$  is the unit vector of the  $x_i$ -axis, and  $\eta$  is the undeformed arm distance along this vector between the origin of the coordinate system ( $O_i$ ) and the arbitrary differential element  $Q$ . Also,  $\mathbf{r}_{ij}$  is the vector of elastic deformation mode shapes which denote the  $j$ 'th longitudinal/transverse mode shape of the  $i$ 'th link. To describe the position of the differential element  $Q$  in absolute terms, recursive equations are utilized in a way that the position of a said element relative to the origin of the coordinate system ( $O_i$ ) and then relative to the coordinate system attached to the platform is obtained. This is described as

$${}^i\mathbf{r}_Q = {}^i\mathbf{r}_{Q/O_i} + {}^i\mathbf{r}_{O_i} \quad \text{where } {}^i\mathbf{r}_{O_i} = {}^i\mathbf{R}_{i-1} \left( {}^{i-1}\mathbf{r}_{O_i/O_{i-1}} + {}^{i-1}\mathbf{r}_{O_{i-1}} \right) \quad (2)$$

where finding  ${}^{i-1}\mathbf{r}_{O_i/O_{i-1}}$  only requires considering the position of the differential element  $Q$  at the end of  $(i-1)$ 'th link. Also, the matrix  ${}^i\mathbf{R}_{i-1}$  is the rotation matrix between the origin of the coordinate system attached

$${}^i\dot{\mathbf{r}}_Q = {}^i\mathbf{R}_{i-1} \left( {}^{i-1}\boldsymbol{\omega}_{i-1} \times {}^{i-1}\mathbf{r}_{O_i/O_{i-1}} + {}^{i-1}\ddot{\mathbf{r}}_{O_{i-1}} \right) \quad (6)$$

The acceleration vector of the differential element  $Q$  using absolute and recursive explanation is written as

$${}^i\ddot{\mathbf{r}}_Q = {}^i\ddot{\mathbf{r}}_{O_i} + {}^i\ddot{\mathbf{r}}_{Q/O_i} + {}^i\dot{\boldsymbol{\omega}}_i \times {}^i\mathbf{r}_{Q/O_i} + 2 {}^i\dot{\boldsymbol{\omega}}_i \times {}^i\mathbf{r}_{Q/O_i} + {}^i\boldsymbol{\omega}_i \times \left( {}^i\boldsymbol{\omega}_i \times {}^i\mathbf{r}_{Q/O_i} \right) \quad (7)$$

where the vector  ${}^i\dot{\boldsymbol{\omega}}_i$  shows the angular acceleration of the  $i$ 'th link as in

## 3. Dynamic modeling of underwater N-link flexible manipulator

In this section, deriving the motion equations of underwater robotic chains involves the calculation of the dynamic interactions between the fluid medium and the robot links obtaining the dynamic equations of the robotic chain by considering these interactions. Therefore, in the first step, the hydrodynamic and hydrostatic effects of the fluid on the robot links are evaluated. These effects are calculated according to the continuum dynamics of the robot's flexible links along their length. The result of these calculations is applied in the dynamic equations of the robotic arm, and the impact of environmental conditions is also considered in its behavior. In comparison to the robotic chain's motion

equations used in air environments, the mentioned interactions forces have several effects which should be categorized base on defined expression for preparing the distinct part of links and fluid medium interactions. Hence, the summation of this categorized expression prepares the precise value for dynamic forces fluid-manipulator interactions.

### 3.1. Dynamic modeling of fluid-manipulator interaction

The model studied in this section is different from previous models in that a flexible robotic arm in a fluid medium is considered (Tarn et al., 1996). As a result, in the first stage, the effect of the fluid-manipulator interaction is considered and related dynamic equations are derived. The hydrodynamic forces created by the movement of robotic arms within the fluid medium are often nonlinear and complex to calculate. Discussions on hydrodynamic forces and their impact on fully-immersed objects have been presented in the studies of Yuh, Foss, and Patel (Antonelli et al., 2008; Goheen, 1991; McMillan et al., 1995; Minoo H Patel, n.d.; Pettersen and Fossen, 2018; Yuh, 1990). These forces are calculated based on an incompressible fluid flow via Navier-Stokes equations. However, these equations rarely arrive at exact solutions, and in certain cases, these forces are modeled approximately in concentrated form for specific applications according to specific assumptions. The effect of these forces is identified as four separate interactions and is later considered in the modeling and simulation of objects immersed in the fluid. These effects include added mass, buoyancy, fluid acceleration, and lift and drag forces. Unfortunately, the mentioned effects are not limited to a specified external load and they do not act as concentrated forces when the manipulator with flexible links has been used. In following the hydrostatic and hydrodynamic effects of the fluid medium on the flexible manipulator have been illustrated.

#### 3.1.1. Hydrostatic and hydrodynamic effects of fluid on the flexible-link manipulator

Fig. 3 shows the hydrostatic and hydrodynamic forces applied to the  $i$ 'th link of the rigid robotic arm in the fluid medium. The harmonic motion of an object in a fluid generates a reaction force due to pressure as well as a corresponding moment of inertia described as a linear

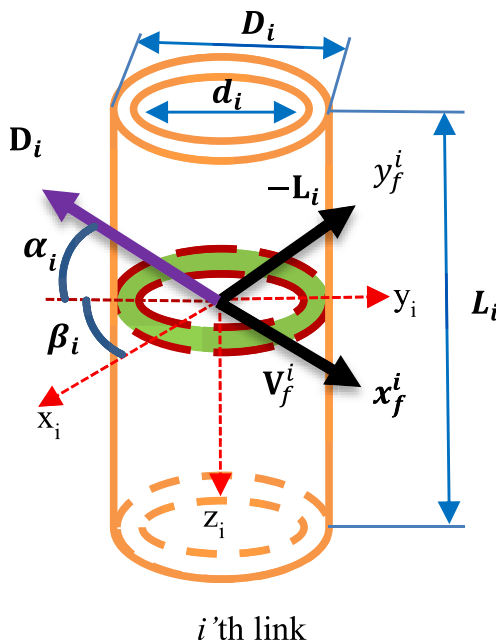


Fig. 3. Nonlinear hydrostatic and hydrodynamic forces exerted to the  $i$ 'th link of the robotic arm.

function of object acceleration. These forces are considered as added mass and added moment of inertia in the dynamic equations of the multi-body. The fluid friction on identical elements at the same depth is considered in the form of load exerted at the pressure center of the links of the robotic arm.

These are drag's forces and act in the direction of velocity flow. Thus, according to Fig. 3, the resulting vortex causes an oscillating force in both the drag direction and perpendicular to it (i.e., the lift). If the fluid flow coordinate system is defined as  $x_f^i, y_f^i, z_f^i$ , then the flow velocity ( $V_f$ ) lies along with its  $x_f^i$ -axis. In this fluid flow coordinate system connected to the  $i$ 'th link, the drag ( $D_i$ ) and lift ( $L_i$ ) are along the  $x_f^i$ - and  $y_f^i$ -axis, respectively.

The conversion matrix between the fluid flow coordinate system and the coordinate system connected to the  $i$ 'th link is defined by defining two-directional angles. The attachment angle  $\alpha$  as well as the lateral slip angle  $\beta$  are the two-directional angles specified in Fig. 3. These two angles are determined by the planar rotation of  $\alpha$  about the  $y_i$ -axis and rotating  $\beta$  along the  $z_i$ -axis. These results are used in the conversion matrix  $R_f^i$  between the coordinate system attached to the  $i$ 'th link and the fluid-flow coordinate system  $f$ .

$$R_f^i = R_z(-\beta)R_y(\alpha) \quad (9)$$

$$R_f^i = \begin{bmatrix} \cos(\beta)\cos(\alpha) & \sin(\beta) & \cos(\beta)\sin(\alpha) \\ -\sin(\beta)\cos(\alpha) & \cos(\beta) & -\sin(\beta)\sin(\alpha) \\ -\sin(\alpha) & 0 & \cos(\alpha) \end{bmatrix} \quad (10)$$

thus, one can define the drag ( $D_i$ ) and lift ( $L_i$ ) forces in the coordinate system attached to the  $i$ 'th link as in

$$F_d^i = R_f^i \begin{bmatrix} -D_i \\ 0 \\ L_i \end{bmatrix} \quad (11)$$

since the drag force depends on the fluid density, it represents the most important hydrodynamic parameter that changes the system behavior based on its velocity.

$$D_i = D_s^i V_r^i + D_r^i |V_r^i| V_r^i + D_q^i (V_r^i)^T V_r^i + O((V_r^i)^3) \quad (12)$$

where the terms  $D_s^i$ ,  $D_r^i$  and  $D_q^i$  are drag coefficients and  $V_r^i$  is the one-dimensional velocity of the fluid relative to the  $i$ 'th link of the robotic manipulator. The third term of Equation (12) is neglected owing to the higher order of its components, the symmetry of the link cross-section, and the smaller value compared with other terms of lower order. The linear terms include the surface friction which demonstrates the drag and lift forces as second-order terms. The relative velocity between the fluid and the  $i$ 'th link is described as

$$V_r^i = \dot{r}_C - V_f R_f^i \dot{r}_f \quad (13)$$

where  $\dot{r}_C$  is the translational velocity of the mass center of the  $i$ 'th link of robotic manipulator found from Equation (6), and  $V_f$  is the flow velocity along the  $x_f$ -axis. In addition, the coefficient  $D_r^i$  in Equation (12) is obtained by considering the mentioned assumptions in the form

$$D_r^i = \frac{1}{2} \rho C_D (R_n K_C \alpha_i) A^i(\alpha_i) \quad (14)$$

where  $C_D$  is the drag coefficient,  $A^i(\alpha_i)$  is the projection of the rigid body surface,  $\alpha_i$  is the attack angle,  $R_n$  is the Reynolds number and  $K_C$  is the Keulegan-Carpenter number. The vortex-induced force along the drag is disregarded as it is smaller than  $D_r^i |V_r| V_r$ . Although evaluating the drag effect is simple, the real challenge is computing its coefficients. The amount of lift force is found from

$$L_i = \frac{1}{2} \rho C_L (R_n K_C \alpha_i) A^i(\alpha_i) \cos(2\pi f_r t + \gamma) \quad (15)$$

where  $C_L$  is the lift coefficient, and  $f_r$  is the vortex frequency equal to  $f_r = \frac{S_r + V_f}{d}$  in which  $S_r$  is the Strouhal number. Also,  $\gamma$  is the phase angle that varies along the longitudinal axis of the link. As the manipulator links move through the fluid, the dynamic effects of rotational damping, buoyancy force, and flow pressure on the manipulator links are calculated separately. The moment of inertia due to fluid damping ( $\mathbf{T}_{rd}^i$ ) is a function of the angular velocity of the  $i$ 'th link of a robotic manipulator, angle of attack, and lateral slip angle. Therefore, in general, it is reasonable to assume that the moment of inertia due to fluid damping is a linear function of the angular velocity of manipulator links. The buoyancy force ( $\mathbf{b}^i$ ) is the restoring force generated from fluid displaced by manipulator links. Moreover, the attack force is applied to the center of buoyancy of the link and is equivalent to the amount of displaced fluid. The fluid flow pressure ( $\mathbf{T}_d^i$ ) is applied to the manipulator links and is a function of the velocity of manipulator links relative to the fluid. In the following, the effect of the angular velocity of the robotic arm inside the fluid is investigated.

$$\mathbf{T}_{rd_x}^i = \frac{1}{4} \rho V_r d_x C_{ip}(\alpha, \beta, R_n) \omega_x^i \quad (16)$$

$$\mathbf{T}_{rd_y}^i = \frac{1}{4} \rho V_r d_y C_{mq}(\alpha, \beta, R_n) \omega_y^i \quad (17)$$

$$\mathbf{T}_{rd_z}^i = \frac{1}{4} \rho V_r d_z C_{nr}(\alpha, \beta, R_n) \omega_z^i \quad (18)$$

Thus, the vector of rotational damping due to the fluid moment of inertia is described as

$$\mathbf{T}_{rd}^i = \begin{bmatrix} \mathbf{T}_{rd_x}^i & \mathbf{T}_{rd_y}^i & \mathbf{T}_{rd_z}^i \end{bmatrix}^T \quad (19)$$

where the coefficients of angular derivatives, i.e.,  $C_{ip}$ ,  $C_{mq}$  and  $C_{nr}$  are dimensionless, and  $d_x$ ,  $d_y$  and  $d_z$  are predetermined lengths. To calculate the fluid flow pressure, one should use

$$\mathbf{T}_d^i = \tilde{\mathbf{V}}_r [diag(A_{11}, A_{22}, A_{33})] \mathbf{V}_r \quad (20)$$

The effect of fluid flow can be observed in robotic manipulators with non-circular cross-sections. To keep the desired depth of the underwater robot, its center of buoyancy and center of mass should coincide. The buoyancy force of the robotic manipulator when placed in the fluid is obtained as

$$\mathbf{b}_i = \rho g \nabla_i \quad (21)$$

where  $\nabla_i$  represents the volumetric change of the fluid as a result of the motion of  $i$ 'th link in the robotic manipulator, and  $g$  is the gravitational acceleration.

### 3.2. Derivation of motion equations of underwater flexible manipulator

In the first step of the recursive Gibbs-Appell formulation (Korayem et al., 2019) (Fig. 4), the Gibbs function of the system is found in view of acceleration vectors, potential energy, and Rayleigh dissipation function. For systems that include non-conservative forces, their effect must be considered in the Rayleigh dissipation function. In this regard, the main difference appeared in the Non-conservative forces which should be kept in accounts as Gibbs and dissipation functions. while they were not considered in the previous manipulators for the systems which are work in the air environments.

#### 3.2.1. Gibbs function of underwater robotic chain

The Gibbs function of the underwater robotic system for the  $i$ 'th flexible link consists of three main parts: (1) the Gibbs function of the elastic arm ( $S_{L_i}$ ), (2) the Gibbs function due to the added mass and added moment of inertia ( $S_{AL_i}$ ) which is implemented the effects of surrounding fluid on the parts acceleration energy considered as Gibbs functions, and (3) the Gibbs function due to the mass of the motors and the

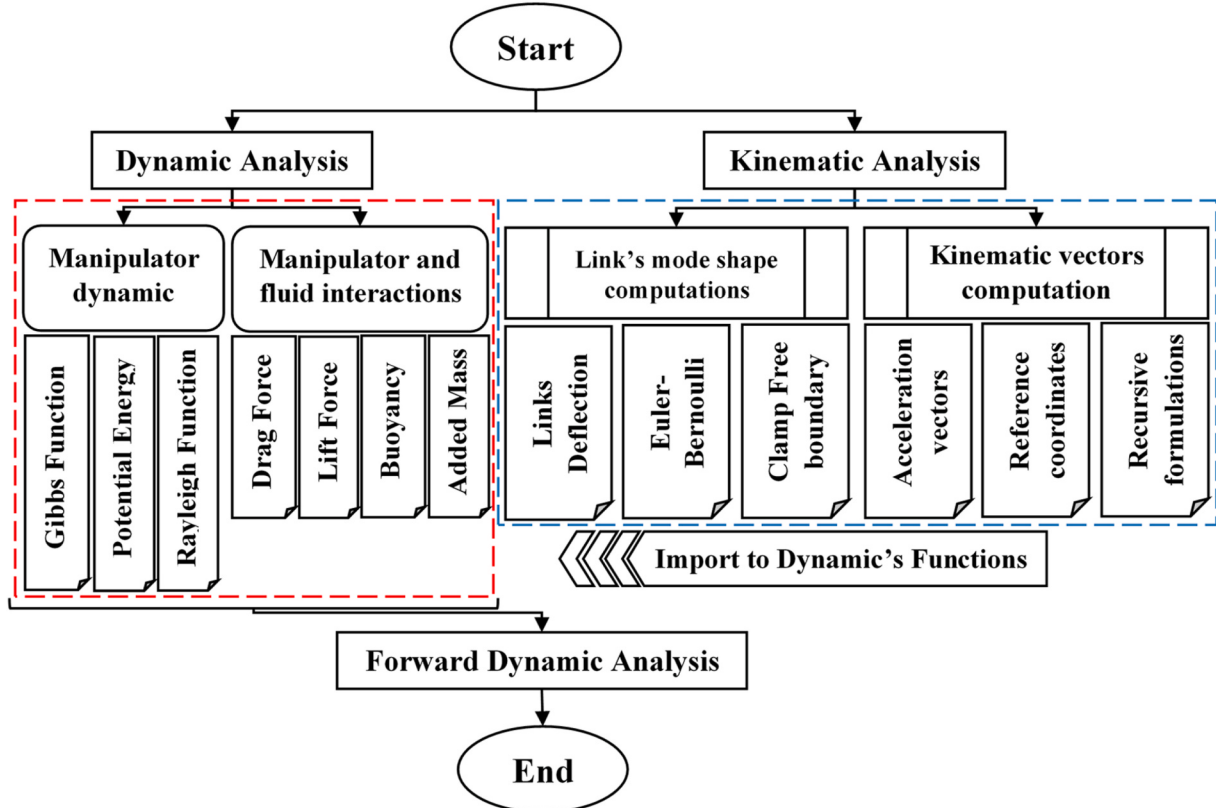


Fig. 4. Flowchart of recursive Gibbs-Appell formulation.

concentrated mass of the gripper ( $S_{P_i}$ ). Therefore, to calculate the Gibbs function, the differential element  $Q$  as shown in Fig. 1 is considered on the  $i$ 'th link of the robotic manipulator. The differential element  $Q$  can experience rigid-body rotation and elastic deformation at any time. As a result, the Gibbs function for the differential element  $Q$  is expressed as

$$dS_{L_i} = \frac{1}{2} \mu_i(\eta) \left( \dot{\mathbf{r}}_Q^T \cdot \dot{\mathbf{r}}_Q \right) d\eta \quad (22)$$

$$dS_{AL_i} = \frac{1}{2} C_m \mu_{A_i}(\eta) \left( \dot{\mathbf{r}}_Q^T \cdot \dot{\mathbf{r}}_Q \right) d\eta \quad (23)$$

$$S_{P_i} = \frac{1}{2} M_{m_i} \left( \dot{\mathbf{r}}_{O_{i+1}}^T \cdot \dot{\mathbf{r}}_{Q_{i+1}} \right) \quad (24)$$

where  $\mu_i(\eta)$  is the mass per unit length,  $\mu_{A_i}(\eta)$  is the volumetric mass per unit length considering the density of the fluid surrounding the manipulator (used to calculate the added mass of the  $i$ 'th link),  $M_{m_i}$  is the motor mass of the  $i$ 'th joint of robotic manipulator at the location of the  $(i+1)$ 'th coordinate system, and  $C_m$  is the hydrodynamic coefficient of added mass and moment of inertia. Next, by integrating along the arm length and summing the values obtained for each link, the Gibbs function of the entire manipulator system is calculated as

$$S = \sum_{i=1}^n \left( \int_0^{L_i} dS_{L_i} + \int_0^{L_i} dS_{AL_i} + S_{P_{i+1}} \right) \quad (25)$$

Therefore, the final Gibbs function is written in expanded form as

$$\begin{aligned} S = & \sum_{i=1}^n \frac{1}{2} (B_{0i}) \ddot{\mathbf{r}}_{O_i}^T \ddot{\mathbf{r}}_{O_i} + \ddot{\mathbf{r}}_{O_i}^T \mathbf{B}_{1i} - 2 \ddot{\mathbf{r}}_{O_i}^T (B_{2i})^i \mathbf{\omega}_i - \\ & \ddot{\mathbf{r}}_{O_i}^T (B_{3i})^i \mathbf{\omega}_i - \ddot{\mathbf{r}}_{O_i}^T \tilde{\mathbf{\omega}}_i (B_{3i})^i \mathbf{\omega}_i + \frac{1}{2} B_{4i} - 2^i \mathbf{\omega}_i^T \mathbf{B}_{5i} + \dot{\mathbf{\omega}}_i^T \mathbf{B}_{6i} - \\ & \dot{\mathbf{\omega}}_i^T (B_{7i})^i \mathbf{\omega}_i + 2 \dot{\mathbf{\omega}}_i^T (B_{8i})^i \mathbf{\omega}_i + \frac{1}{2} \dot{\mathbf{\omega}}_i^T (B_{9i})^i \dot{\mathbf{\omega}}_i + \dot{\mathbf{\omega}}_i^T \tilde{\mathbf{\omega}}_i (B_{9i})^i \mathbf{\omega}_i + \\ & \frac{1}{2} (M_{m_i}) \ddot{\mathbf{r}}_{O_{i+1}}^T \ddot{\mathbf{r}}_{O_{i+1}} + \text{irrelevant terms} \end{aligned} \quad (26)$$

where  $\dot{\tilde{\mathbf{\omega}}}_i$  is the skew-symmetric matrix of the angular velocity of  $i$ 'th arm, and the last term includes those parameters that are no functions of Quasi-accelerations. Hence, they are eliminated as they have no specific role in the dynamic equations. The mentioned parameters in Equation (26) are presented in Appendix A.

### 3.2.2. Potential energy of the underwater flexible robotic chain

To calculate the system potential energy, the effect of three sources of potential energy is considered: (1) elastic deformation of arms, (2) Earth's gravity, and (3) buoyancy due to the interactions of the fluid environment. Owing to the inherent symmetry of flexible links in the structure of robotic chains, the effect of gravity and buoyancy is considered by applying an acceleration to the manipulator platform according to Equation (21), i.e.,  $\frac{\rho g}{m_i} \mathbf{g}$  for the buoyancy and  $\mathbf{g}$  for the gravitational acceleration. Both force effects are applied along the Z-axis of the reference frame XYZ.

The strain potential energy stored in the  $i$ 'th link of a robotic manipulator, assuming Euler-Bernoulli Beam Theory (EBT), which is used to compute the mode shapes of manipulator links is described as

$$V_{L_i} = \frac{1}{2} \int_0^{L_i} \left[ E_i I_{yi} \left( \frac{\partial \varphi_{yi}}{\partial \eta} \right)^2 + E_i I_{zi} \left( \frac{\partial \varphi_{zi}}{\partial \eta} \right)^2 + E_i A_i \left( \frac{\partial r_{ij}}{\partial \eta} \right)^2 + G_i I_{xi} \left( \frac{\partial \varphi_{xi}}{\partial \eta} \right)^2 \right] d\eta \quad (27)$$

where  $E_i$  is the modulus of elasticity,  $\mathbf{I}$  is the arm moment of inertial about the axes  $x$ ,  $y$ , and  $z$ , and  $A_i$  is the cross-section of the  $i$ 'th link.

Hence, the total potential energy of the system is written as

$$V_L = \frac{1}{2} \sum_{i=1}^n \sum_{j=1}^{m_i} \sum_{k=1}^{m_i} \delta_{ij}(t) \delta_{ik}(t) \mathbf{K}_{ijk}$$

where

$$\mathbf{K}_{ijk} = \int_0^{L_i} \left[ E_i I_{yi} \frac{\partial \varphi_{yi}}{\partial \eta} \frac{\partial \varphi_{yik}}{\partial \eta} + E_i I_{zi} \frac{\partial \varphi_{zi}}{\partial \eta} \frac{\partial \varphi_{zik}}{\partial \eta} + E_i A_i \frac{\partial r_{ij}}{\partial \eta} \frac{\partial r_{ik}}{\partial \eta} + G_i I_{xi} \frac{\partial \varphi_{xi}}{\partial \eta} \frac{\partial \varphi_{xik}}{\partial \eta} \right] d\eta \quad (28)$$

### 3.2.3. Rayleigh dissipation function of underwater flexible robotic chain

Usually, non-conservative forces can decrease the system energy in dynamic systems. When using a flexible robotic manipulator in a fluid, in addition to structural damping, drag and lift forces are also among the non-conservative forces that should be taken into account when calculating the Rayleigh dissipation function. In this regard, the vibratory energy is dissipated in the mechanical systems for widespread reasons. It may contain a complex or a simple component mechanical system (Kabe and Sako, 2020). Hence, the damping mechanism can be mainly divided into three categories including:

- a) Solid interactions dissipation.
- b) Fluid medium interactions dissipation.
- c) The interface between solids or solid and fluid.

The first one which is common between the manipulator system perform in air and fluid environments are the internal or material damping refers to inherent energy dissipation during the motion or deformation of the manipulator's links.

**3.2.3.1. Rayleigh dissipation function due to structural damping.** The structural damping may be found by assuming it in the form of viscous damping. The Rayleigh dissipation function due to the structural damping of the flexible robotic manipulator according to the Kelvin-Voigt model is expressed as

$$\begin{aligned} D_{L_i} = & \frac{1}{2} \int_0^{L_i} \Upsilon \left[ \left( \frac{\partial v_i}{\partial t} \right)^2 + \left( \frac{\partial w_i}{\partial t} \right)^2 \right] d\eta \\ & + \frac{1}{2} \int_0^{L_i} K_{v_i} \left[ I_{zi} \left( \frac{\partial^3 v_i}{\partial \eta^2 \partial t} \right)^2 + I_{yi} \left( \frac{\partial^3 w_i}{\partial \eta^2 \partial t} \right)^2 \right] d\eta \end{aligned} \quad (29)$$

where  $K_{v_i}$  is the Kelvin-Voigt damping coefficient for the  $i$ 'th arm, and  $\Upsilon$  is the damping coefficient of its surrounding medium which is chosen according to the working environment of the robotic arm. Substituting the values of deformation in Equation (29) based on the AMM allows one to derive the final form of Rayleigh dissipation function due to the structural damping as in

$$D_L = \frac{1}{2} \sum_{i=1}^n \sum_{j=1}^{m_i(i)} \sum_{k=1}^{m_i(i)} \dot{\delta}_{ij}(t) \dot{\delta}_{ik}(t) D_{ijk}$$

where

$$D_{ijk} = \int_0^{L_i} \gamma (r_{yij} r_{yik} + r_{zij} r_{zik}) d\eta + \int_0^{L_i} K_{v_i} \left( I_{zi} \frac{\partial^2 r_{yij}}{\partial \eta^2} \frac{\partial^2 r_{yik}}{\partial \eta^2} + I_{yi} \frac{\partial^2 r_{zij}}{\partial \eta^2} \frac{\partial^2 r_{zik}}{\partial \eta^2} \right) d\eta \quad (30)$$

**3.2.3.2. Rayleigh dissipation function due to lift and drag.** The effect of non-conservative forces caused by drag and lift on the robotic arm is shown in Equation (11). Thus, to calculate the reduced energy in the Rayleigh dissipation function, the work done by drag and lift must be calculated. The computed dissipation systems from the work done by the

robotic arm to displace the surrounding fluid around it. On the other hand, the amount of Rayleigh dissipation function can be found by calculating the fluid kinetic energy. Thus, the Rayleigh dissipation function due to drag and lift is written as

$$D_{d_i}^d = \frac{1}{2} \int_0^{L_i} \rho C_d d_i \eta_i \left( \dot{\mathbf{r}}_Q^T \cdot \dot{\mathbf{r}}_Q \right) d\eta_i \quad (31)$$

$$D_{d_i}^L = \frac{1}{2} \int_0^{L_i} \rho C_L d_i \eta_i \left( \dot{\mathbf{r}}_Q^T \cdot \dot{\mathbf{r}}_Q \right) d\eta_i \quad (32)$$

By summing the obtained values for each link, the total Rayleigh dissipation function of the system can be expressed as

$$\begin{aligned} D_d &= \sum_{i=1}^n \left( D_{d_i}^L + D_{d_i}^d \right) = \sum_{i=1}^n \left( \frac{1}{2} \int_0^{L_i} \rho (C_d + C_L) d_i \eta_i \left( \dot{\mathbf{r}}_Q^T \cdot \dot{\mathbf{r}}_Q \right) d\eta_i \right) = \\ &\sum_{i=1}^n \frac{1}{2} (W_{0i}) \dot{\mathbf{r}}_{O_i}^T \dot{\mathbf{r}}_{Q_i} + \dot{\mathbf{r}}_{O_i}^T \mathbf{W}_{1i} - \dot{\mathbf{r}}_{O_i}^T W_{2i} \dot{\mathbf{w}}_i + \frac{1}{2} W_{3i} + \\ &\frac{1}{2} \dot{\mathbf{w}}_i^T (W_{4i}) \dot{\mathbf{w}}_i \end{aligned} \quad (33)$$

where

$$W_{0i} = \int_0^{L_i} \rho (C_d + C_L) d_i \eta_i d\eta_i; \quad (34)$$

$${}^i \mathbf{W}_{1i} = \sum_{j=1}^{m(i)} \delta_{ij} T_{1ij}; \quad (35)$$

$$W_{2i} = \sum_{j=1}^{m(i)} \dot{\delta}_{ij} \tilde{\mathbf{T}}_{1ij}; \quad (36)$$

$$W_{3i} = \sum_{j=1}^{m(i)} \dot{\delta}_{ij} \left( \sum_{k=1}^{m(i)} \dot{\delta}_{ik} T_{2ijk} \right); \quad (37)$$

$$W_{4i} = T_{3i} + \sum_{j=1}^{m(i)} \delta_{ij} \left( T_{4ij}^T + \kappa_{ij} \right) \quad (38)$$

The coefficients of Equation (36) are written as

$$\mathbf{T}_{1ij} = \int_0^{L_i} \rho (C_d + C_L) d_i \eta_i \mathbf{r}_{ij} d\eta_i; \quad (39)$$

$$\tilde{\mathbf{T}}_{1ij} = \int_0^{L_i} \rho (C_d + C_L) d_i \eta_i \tilde{\mathbf{r}}_{ij} d\eta_i \quad (40)$$

$$\mathbf{T}_{2ijk} = \int_0^{L_i} \rho (C_d + C_L) d_i \eta_i \mathbf{r}_{ij}^T \cdot \mathbf{r}_{ij} d\eta_i; \quad (41)$$

$$T_{3i} = \int_0^{L_i} \rho (C_d + C_L) d_i \eta_i^3 \tilde{\mathbf{x}}_i^T \tilde{\mathbf{x}}_i d\eta_i \quad (42)$$

$$\mathbf{T}_{4ij} = \int_0^{L_i} \rho (C_d + C_L) d_i \eta_i^2 \tilde{\mathbf{x}}_i^T \tilde{\mathbf{r}}_{ij} d\eta_i; \quad (43)$$

$$\mathbf{T}_{5ijk} = \int_0^{L_i} \rho (C_d + C_L) d_i \eta_i \tilde{\mathbf{r}}_{ij}^T \tilde{\mathbf{r}}_{ij} d\eta_i \quad (44)$$

$$\kappa_{ij} = \mathbf{T}_{4ij} + \sum_{k=1}^{m(i)} \delta_{ik} \mathbf{T}_{5ijk}; \quad (45)$$

Therefore, the system Rayleigh dissipation function is the sum of Equations 30 and 33.

### 3.2.4. Derivation of inverse dynamic equations of underwater flexible manipulator

To derive different terms of the equation of motion, computational evaluations are performed on the previously-obtained Gibbs function, potential energy, and Rayleigh dissipation function according to Fig. 4. To this aim, the inverse dynamic form of recursive Gibbs-Appell formulation is used according to

$$\frac{\partial S}{\partial \dot{\theta}_j} + \frac{\partial D}{\partial \dot{\theta}_j} + \frac{\partial V}{\partial \dot{\theta}_j} = \tau_j \quad j = 1, \dots, n \quad (46)$$

where the vector  $\tau$  represents the torques of the robot's revolute joints. Different terms of Equation (46) are found by taking the derivative of scalar values as in what follows.

#### 3.2.4.1. Derivative of gibbs function with respect to generalized quasi-accelerations

$$\frac{\partial S}{\partial \ddot{\theta}_j} = \sum_{i=j+1}^n \frac{\partial \dot{\mathbf{r}}_{O_i}^T}{\partial \ddot{\theta}_j} {}^i \mathbf{S}_i + \sum_{i=j}^n \frac{\partial \dot{\mathbf{o}}_{iL}^T}{\partial \ddot{\theta}_j} {}^i \mathbf{T}_{ii}; \quad (47)$$

$$\frac{\partial S}{\partial \ddot{\delta}_{jf}} = \sum_{i=j+1}^n \frac{\partial \dot{\mathbf{r}}_{O_i}^T}{\partial \ddot{\delta}_{jf}} {}^i \mathbf{S}_i + \sum_{i=j+1}^n \frac{\partial \dot{\mathbf{o}}_{iL}^T}{\partial \ddot{\delta}_{jf}} {}^i \mathbf{T}_i + Q_{jf}; \quad (48)$$

in which

$${}^i \mathbf{S}_i = (B_{0i}) \dot{\mathbf{r}}_{O_i} + ({}^i \mathbf{B}_{1i}) - 2(B_{2i}) \dot{\mathbf{w}}_i - (B_{3i}) \dot{\mathbf{w}}_i - \tilde{\mathbf{w}}_i (B_{3i}) \dot{\mathbf{w}}_i \quad (49)$$

$${}^i \mathbf{T}_i = (B_{3i}) \dot{\mathbf{r}}_{O_i} + ({}^i \mathbf{B}_{6i}) + 2(B_{8i}) \dot{\mathbf{w}}_{6i} + (B_{9i}) \dot{\mathbf{w}}_i + \tilde{\mathbf{w}}_i (B_{9i}) \dot{\mathbf{w}}_i \quad (50)$$

$$Q_{jf} = \sum_{k=1}^{m_j} \ddot{\delta}_{jk} (C_{3jk} + C_{7jk}) - 2 \dot{\mathbf{o}}_j^T \sum_{k=1}^{m_j} \dot{\delta}_{jk} \mathbf{C}_{4jk} - {}^j \mathbf{o}_j^T \cdot \beta_{jf} {}^j \mathbf{o}_j + {}^j \mathbf{r}_{O_j}^T \mathbf{C}_{1jf} + {}^j \mathbf{o}_j^T \cdot \mathbf{a}_{jf} \quad (51)$$

#### 3.2.4.2. Derivative of potential energy with respect to generalized coordinates

$$\frac{\partial V}{\partial \dot{\theta}_j} = 0; \quad (52)$$

$$\frac{\partial V}{\partial \dot{\delta}_{jf}} = \sum_{k=1}^{m_j} \dot{\delta}_{jk}(t) \mathbf{K}_{jkf}; \quad (53)$$

#### 3.2.4.3. Derivative of Rayleigh dissipation function with respect to generalized quasi-velocities

$$\frac{\partial D}{\partial \dot{\theta}_j} = \frac{\partial (D_d + D_L)}{\partial \dot{\theta}_j} = \sum_{i=j+1}^n \frac{\partial \dot{\mathbf{r}}_{O_i}}{\partial \dot{\theta}_j} {}^i \mathbf{S}'_i + \sum_{i=j}^n \frac{\partial \dot{\mathbf{o}}_{iL}^T}{\partial \dot{\theta}_j} {}^i \mathbf{T}'_i \quad (54)$$

$$\frac{\partial D}{\partial \dot{\delta}_{jf}} = \frac{\partial (D_d + D_L)}{\partial \dot{\delta}_{jf}} = \sum_{k=1}^{m_j} \dot{\delta}_{jk}(t) \mathbf{D}_{jkf} + \sum_{i=j+1}^n \frac{\partial \dot{\mathbf{r}}_{O_i}}{\partial \dot{\delta}_{jf}} {}^i \mathbf{S}'_i + \sum_{i=j+1}^n \frac{\partial \dot{\mathbf{o}}_{iL}^T}{\partial \dot{\delta}_{jf}} {}^i \mathbf{T}'_i + Q'_{jf} \quad (55)$$

where

$${}^i \mathbf{S}'_i = (W_{0i}) \dot{\mathbf{r}}_{O_i} + ({}^i \mathbf{W}_{1i}) - (W_{2i}) \dot{\mathbf{w}}_i \quad (56)$$

$${}^i\dot{\mathbf{T}}_i' = (W_{2i}){}^i\dot{\mathbf{r}}_{O_i} + (W_{4i}){}^i\omega_i \quad (57)$$

$$\dot{\mathbf{Q}}_{if}' = \sum_{k=1}^{m_j} \dot{\delta}_{if} T_{2jk} - {}^j\dot{\mathbf{r}}_{O_j} \cdot \tilde{\mathbf{T}}_{1jf} {}^j\omega_j + {}^j\dot{\mathbf{r}}_{O_j} \cdot \mathbf{T}_{1jf} \quad (58)$$

Substituting the obtained values in Equation (36), two sets of inverse dynamic equations are obtained as in

$$\frac{\partial S}{\partial \ddot{\theta}_j} + \frac{\partial D}{\partial \dot{\theta}_j} + \frac{\partial V}{\partial \theta_j} = \tau_j \quad j = 1, \dots, n \quad (59)$$

$$\frac{\partial S}{\partial \ddot{\delta}_j} + \frac{\partial D}{\partial \dot{\delta}_j} + \frac{\partial V}{\partial \delta_j} = 0 \quad j = 1, \dots, n \quad (60)$$

### 3.2.5. Derivation of the forward dynamic equations of the underwater robotic system

By considering Equations (59) and (60), the general form of the forward dynamic equations is concluded in which the terms that are functions of the second derivative of generalized coordinates are placed on the left-hand side along with their associated coefficients and form the system inertia matrix ( $\mathbf{I}(\Theta, \dot{\Theta})$ ). Other terms are moved to the right-hand side and form the vector of forces and remaining terms. Accordingly, the vector  $\mathbf{Re}(\Theta, \dot{\Theta})$  and the vector of input torques  $\Gamma$  constitute the terms on the right-hand side of the forward dynamic equations as

$$\mathbf{I}(\Theta, \dot{\Theta})\ddot{\Theta} = \mathbf{Re}(\Theta, \dot{\Theta}) + \Gamma \quad (61)$$

The elements of the inertia matrix in Equation (61) consist of terms written as functions of kinematic variables of previous links (i.e., recursive form). Next,  $\dot{r}_{O_i}$  and  $\dot{\omega}_i$  (Equations (5) and (8)) must be separated based on the terms that contain generalized quasi-accelerations. The outcomes of this separation are  $\ddot{r}_{O_{si}}$  and  $\dot{\omega}_{si}$ , which must be withdrawn from their recursive form and rewritten as a summation form. The obtained values are differentiated with respect to the generalized quasi-accelerations to be replaced in the elements of the inertia matrix.

$$\frac{\partial^i \dot{\omega}_i}{\partial \ddot{\theta}_j} = {}^i\mathbf{R}_j {}^j\mathbf{z}_j; \frac{\partial^i \dot{\omega}_i}{\partial \ddot{\delta}_{if}} = {}^i\mathbf{R}_j \theta_{if}(l_j) \quad (62)$$

$$\frac{\partial^i \ddot{r}_{O_i}}{\partial \ddot{\theta}_j} = {}^i\mathbf{R}_j {}^j\mathbf{z}_j \times {}^i\mathbf{r}_{O_i/O_j}; \frac{\partial^i \ddot{r}_{O_i}}{\partial \ddot{\delta}_{if}} = {}^i\mathbf{R}_j \mathbf{r}_{if}(l_j) + {}^i\mathbf{R}_j \theta_{if}(l_j) \times {}^i\mathbf{r}_{O_i/O_{j+1}}; \quad (63)$$

$$\frac{\partial^i \dot{\omega}_i}{\partial \theta_j} = {}^i\mathbf{R}_j {}^j\mathbf{z}_j; \frac{\partial^i \dot{\omega}_i}{\partial \delta_{if}} = {}^i\mathbf{R}_j \theta_{if}(l_j) \quad (64)$$

$$\frac{\partial^i \dot{r}_{O_i}}{\partial \theta_j} = {}^i\mathbf{R}_j {}^j\mathbf{z}_j \times {}^i\mathbf{r}_{O_i/O_j}; \frac{\partial^i \dot{r}_{O_i}}{\partial \delta_{if}} = {}^i\mathbf{R}_j \mathbf{r}_{if}(l_j) + {}^i\mathbf{R}_j \theta_{if}(l_j) \times {}^i\mathbf{r}_{O_i/O_{j+1}}; \quad (65)$$

**3.2.5.1. System inertia matrix ( $\mathbf{I}(\Theta, \dot{\Theta})$ ).** The left-hand side of the inverse dynamic equations (i.e., Equations (59) and (60)) are rewritten as recursive form after substituting Equation (62) – (65), followed by grouping based on the quasi-acceleration coefficients. As a result, the system inertia matrix is formed. This matrix contains the following elements.

Quasi-acceleration coefficients of the coupled equation of revolute joint

$$\left( \begin{array}{l} \sum_{k=1}^n {}^j\mathbf{z}_j^T ({}^j\sigma_k - {}^j\psi_k + {}^j\sigma_k' \sigma_k' - {}^j\psi_k') \mathbf{k} \mathbf{z}_k - \sum_{k=1}^{n-1} {}^j\mathbf{z}_j^T \left( {}^jU_k + {}^jU_k' \right) \mathbf{k} \mathbf{z}_k \\ \left( \sum_{k=1}^{n-1} \sum_{t=1}^{m(i)} {}^j\mathbf{z}_j^T ({}^j\sigma_{kt} - {}^j\psi_{kt}) \mathbf{0}_{kt} + \sum_{k=1}^{n-1} \sum_{t=1}^{m(i)} {}^j\mathbf{z}_j^T ({}^j\xi_{kt} + {}^j\gamma_k) \mathbf{r}_{kt} \right) \ddot{q}_k \\ + \left( - \sum_{k=1}^{n-2} \sum_{t=1}^{m(i)} {}^j\mathbf{z}_j^T {}^jU_{k+1} \mathbf{0}_{kt} + \sum_{k=j+1}^n \sum_{t=1}^{m(i)} {}^j\mathbf{z}_j^T \tilde{\mathbf{r}}_{O_k/O_j} {}^j\mathbf{R}_k \mathbf{C}_{1kt} \right. \\ \left. + \sum_{k=j}^n \sum_{t=1}^{m(i)} {}^j\mathbf{z}_j^T {}^j\mathbf{R}_k \alpha_{kt} \right) \ddot{\delta}_{kt} \end{array} \right) \quad (66)$$

**3.2.5.2. Quasi-acceleration coefficients of the coupled equation of deformation.** Due to the symmetry in the system inertia matrix, the coefficient  $\ddot{q}_k$  in Equation (66) is equivalent to the coefficient  $\ddot{\delta}_{kt}$  in the coupled equation of revolute joint.

$$\left( \begin{array}{l} \sum_{k=1}^{n-1} \sum_{t=1}^{m(i)} \mathbf{0}_{if}^T ({}^{j+} \sigma_{kt} - {}^{j+} \psi_{kt}) \mathbf{0}_{kt} - \sum_{k=1}^{n-2} \sum_{t=1}^{m(i)} \mathbf{0}_{if}^T {}^{j+} U_{k+1} \mathbf{0}_{kt} \\ - \sum_{k=1}^{n-1} \sum_{t=1}^{m(i)} \mathbf{r}_{if}^T {}^{j+} \xi_{kt} \mathbf{0}_{kt} - \sum_{k=1}^{n-2} \sum_{t=1}^{m(i)} \mathbf{C}_{1jf}^T \times {}^jW_k \mathbf{0}_{kt} + \sum_{k=1}^{n-1} \sum_{t=1}^{m(i)} \alpha_{if}^T {}^j\mathbf{R}_k \mathbf{0}_{kt} \\ + \sum_{t=1}^{m(i)} C_{4kf} + \sum_{k=1}^{n-1} \sum_{t=1}^{m(i)} \mathbf{0}_{if}^T ({}^{j+} \gamma_k + {}^{j+} \xi_{kt}) \mathbf{r}_{kt} + \sum_{k=j+1}^n \sum_{t=1}^{m(i)} \mathbf{0}_{if}^T {}^j\mathbf{R}_k \alpha_{kt} \\ + \sum_{k=1}^{n-1} \sum_{t=1}^{m(i)} \mathbf{r}_{if}^T {}^j\lambda_k \mathbf{r}_{kt} + \sum_{k=1}^{n-1} \sum_{t=1}^{m(i)} \mathbf{C}_{1jf}^T {}^j\mathbf{R}_k \mathbf{r}_{kt} + \sum_{k=j+1}^n \sum_{t=1}^{m(i)} \mathbf{r}_{if}^T {}^j\mathbf{R}_k \mathbf{C}_{1kt} \\ + \sum_{k=j+2}^n \sum_{t=1}^{m(i)} \mathbf{0}_{if}^T {}^j\tilde{\mathbf{r}}_{O_k/O_{j+1}} {}^j\mathbf{R}_k \mathbf{C}_{1kt} - \sum_{k=1}^{n-2} \sum_{t=1}^{m(i)} r_{if}^T {}^jV_k \mathbf{0}_{kt} \end{array} \right) \ddot{\delta}_{kt} \quad (67)$$

The intermediate coefficients of Equations (66) and (67) are given in Appendix. B.

**3.2.5.3. Vector of forces and remaining terms ( $\mathbf{Re}(\Theta, \dot{\Theta})$ ).** The right-hand side of Equation (61) consists of restoring forces and torques and remaining terms that do not include the generalized quasi-accelerations.

$$\mathbf{Re}_{q_j} = - \sum_{i=j+1}^n \frac{\partial^i \ddot{\mathbf{r}}_{O_i}}{\partial \ddot{\theta}_j} \times {}^i\mathbf{S}_i - \sum_{i=j+1}^n \frac{\partial^i \dot{\omega}_i}{\partial \ddot{\theta}_j} \times {}^iT_i - \sum_{i=j+1}^n \frac{\partial^i \ddot{r}_{O_i}}{\partial \ddot{\theta}_j} \cdot {}^i\mathbf{S}_i' - \sum_{i=j}^n \frac{\partial^i \dot{\omega}_i}{\partial \ddot{\theta}_j} \cdot {}^i\mathbf{T}_i' \quad (68)$$

$$\mathbf{Re}_{\delta_{if}} = \mathbf{Q}_{if} + \mathbf{Q}_{jf}' - \sum_{i=j+1}^n \frac{\partial^i \ddot{\mathbf{r}}_{O_i}}{\partial \ddot{\delta}_{if}} \times {}^i\mathbf{S}_i - \sum_{i=j+1}^n \frac{\partial^i \dot{\omega}_i}{\partial \ddot{\delta}_{if}} \times {}^iT_i - \sum_{i=j+1}^n \frac{\partial^i \ddot{r}_{O_i}}{\partial \ddot{\delta}_{if}} \cdot {}^i\mathbf{S}_i' - \sum_{i=j+1}^n \frac{\partial^i \dot{\omega}_i}{\partial \ddot{\delta}_{if}} \cdot {}^i\mathbf{T}_i' \quad (69)$$

The obtained equations are then rewritten in recursive form.

$$\mathbf{Re}_{q_j} = \mathbf{r}_j - {}^T \mathbf{z}_j^T \times ({}^j\chi_j + {}^j\chi_j') \quad (70)$$

$$\mathbf{Re}_{\delta_{if}} = \mathbf{Q}_{if} + \mathbf{Q}_{jf}' - \mathbf{r}_{if}^T \times ({}^i\Phi_j + {}^i\Phi_j') - \mathbf{0}_{if}^T \times {}^j\mathbf{R}_{j+1} ({}^{j+1}\chi_{j+1} + {}^{j+1}\chi_{j+1}') \quad (71)$$

where

$${}^j\chi_j = {}^j\mathbf{T}_j + \tilde{\mathbf{r}}_{O_{j+1}/O_j} {}^j\Phi_j + {}^j\mathbf{R}_{j+1} {}^{j+1}\chi_{j+1}$$

$$\begin{aligned} {}^j\boldsymbol{\chi}'_j &= {}^j\mathbf{T}'_j + \tilde{\mathbf{r}}_{o_{j+1}/o_j} {}^j\boldsymbol{\varphi}'_j + {}^j\mathbf{R}_{j+1} {}^{j+1}\boldsymbol{\chi}'_{j+1} \\ {}^j\boldsymbol{\varphi}'_j &= {}^j\mathbf{R}_{j+1} \left( {}^{j+1}\mathbf{S}'_{j+1} + {}^{j+1}\boldsymbol{\varphi}'_{j+1} \right) \end{aligned} \quad (72)$$

Thus, by substituting Equations (66) and (67) in inertia matrix ( $\mathbf{I}(\Theta, \dot{\Theta})$ ), and Equations (70) and (71) in the matrix of forces and remaining terms ( $\mathbf{Re}(\Theta, \dot{\Theta})$ ), Equation (61) turns into

$$\begin{bmatrix} I_{11} & \dots & I_{1n} \\ \vdots & \ddots & \vdots \\ I_{n1} & \dots & I_{nn} \end{bmatrix} \begin{Bmatrix} \ddot{\Theta}_1 \\ \vdots \\ \ddot{\Theta}_n \end{Bmatrix} = \begin{Bmatrix} Re_1 \\ \vdots \\ Re_n \end{Bmatrix} + \begin{Bmatrix} \Gamma_1 \\ \vdots \\ \Gamma_n \end{Bmatrix} \quad (73)$$

#### 4. Computer simulations

In this section, computer simulations are conducted for a flexible two-link robot. The elastic links of the robot are modeled based on the mode shapes of the EBT in conjunction with the AMM with two vibration modes. Three different cases are studied: a) examining the effect of water and air, b) comparison of different link elasticities, and c) evaluation of different initial conditions of robot motion.

Fig. 5 shows the two-link flexible robot used in this section. The simulations are planned in such a way that the robot starts moving from a standstill as a result of gravity or the torque applied to the robot joints. In calculating the elastic deformation of the robot links, the mode shapes of a cantilevered EBT are used as in (HAN et al., 1999).

$$\begin{aligned} y_{11} = y_{21} &= \sin(\beta_1 \cdot \eta) - \sinh(\beta_1 \cdot \eta) - 1.3622(\cos(\beta_1 \cdot \eta) - \cosh(\beta_1 \cdot \eta)) \\ y_{12} = y_{22} &= \sin(\beta_2 \cdot \eta) - \sinh(\beta_2 \cdot \eta) - 0.9818(\cos(\beta_2 \cdot \eta) - \cosh(\beta_2 \cdot \eta)) \end{aligned} \quad (74)$$

where  $\beta_1 = \frac{1.8751}{L_1}$  and  $\beta_2 = \frac{4.694}{L_2}$ . The robot links deform along the y direction. The deformation due to the weight of robot links during motion (z direction) is neglected. The simulation conditions and input parameters are defined specifically for that section based on the corresponding assumption. Table 1 presents the structural features of the robot and its surrounding environment that are common to all simulations.

**Table 1**  
Mechanical specifications of the two-link flexible robotic chain.

Parameter	Description	Value
$L_1 = L_2$	Length	1.0m
$r_1 = r_2$	Link radius	0.005m
$E_1 = E_2$	Links Elasticity	$0.7 \times 10^{11} N \cdot m^{-2}$
$k_1 = k_2$	Shear correction factor	5/6
$m_2$	Joints motor mass	0 Kg
$m_3$		0.495Kg
$\mu_1 = \mu_2$	Mass per unit length	$0.1119 \frac{Kg}{m}$
$G_1 = G_2$	Shear modulus	$77 \times 10^9 N \cdot m^{-2}$
$\rho_1 = \rho_2$	Link's Density	$2850 \frac{Kg}{m}$
$K_v$	Kelvin-Voigt coefficient	$2200 \frac{Kg \cdot s}{m}$
$g$	Gravity acceleration	$10 \frac{m \cdot s^{-2}}$

**Table 2**  
Mechanical specifications of the underwater robotic chain.

Parameter	Description	Value
$\rho_w$	Water's Density	$998 \frac{Kg}{m^3}$
$C_d$	Drag coefficient	1.2
$C_l$	Lift coefficient	0.1
$C_m$	Added mass coefficient	2
$\gamma_a$	Air damping coefficient	$0.2 \frac{Kg \cdot s}{m}$
$\gamma_w$	Water damping coefficient	$0.8 \frac{Kg \cdot s}{m}$

#### 4.1. Simulation of robot motion in the fluid/air

In this section, the interaction between the flexible robotic chain and its surrounding fluid is compared to the case where the robot moves in the air. Table 2 shows the mechanical specifications of the flexible robotic chain used for expressing its motion inside water.

The coefficients of this table are calculated assuming robot links of circular cross-section and significant length compared with their cross-section. The simulation starts from a standstill as a result of the torque applied to the joints of the first and second links according to Fig. 6. The

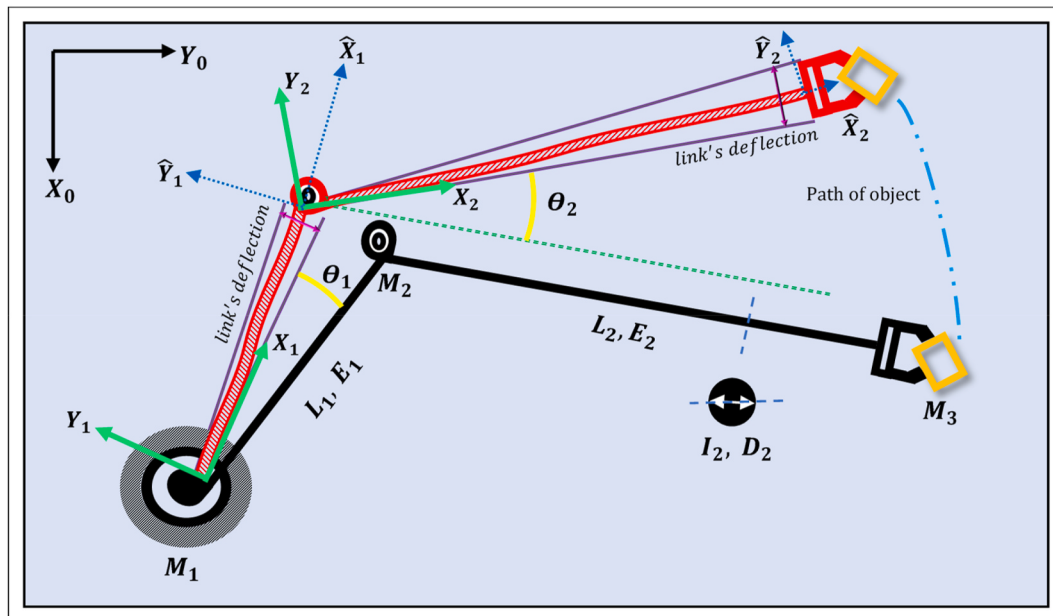


Fig. 5. Underwater two-link flexible robotic chain.

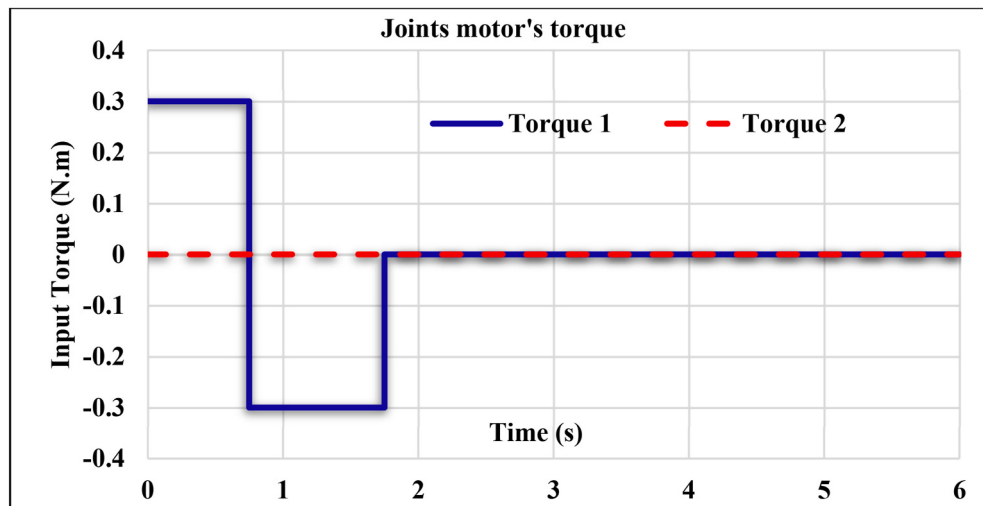


Fig. 6. Exerted torque to the joints of the two-link flexible robotic chain.

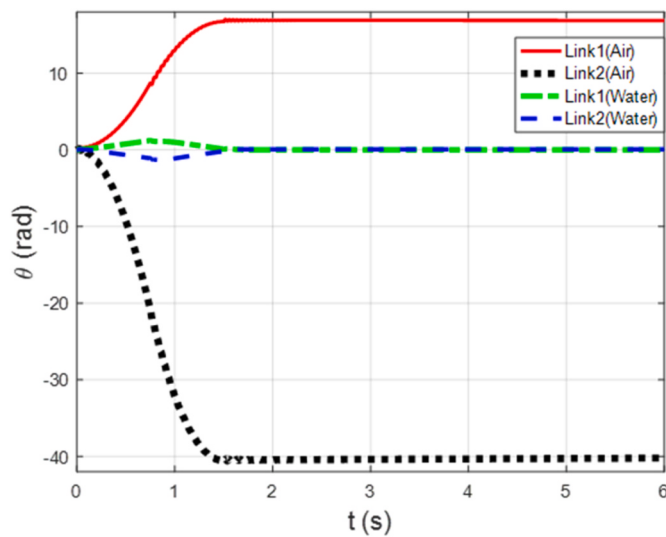


Fig. 7. Joints rotations.

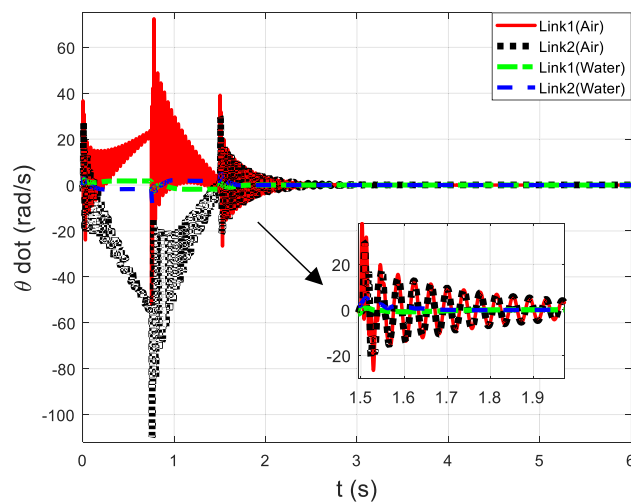


Fig. 8. Joints angular velocities.

initial conditions are  $\{\theta_1 = \theta_2 = \dot{\theta}_{11} = \dot{\theta}_{12} = \dot{\theta}_{21} = \dot{\theta}_{22} = 0\}$ .

Due to the interaction between the arms and the water, the arm's motion continues after the motor torque is removed until it stops. The simulation lasts 6 s.

The angular velocity and angular displacement of the flexible robotic chain are shown in Figs. 7 and 8, respectively. Fig. 7 also displays the effect of the applied torques and their changes on the angular velocity of the robot. At the onset of applying the torque in the air, as well as the instant of changing its direction at 0.75 s and its removal at 1.5 s (according to the diagram of applied torques in Fig. 6), the vibration amplitude of the links increases, although the structural damping and the air damping during movement decrease the vibration amplitude. Nevertheless, previous research indicates that undamped and unstable vibrations are possible consequences of the input torque (Mehrjooee et al., 2019). In contrast, although the application of torque in the water also results in the deformation of the robot's flexible arms, the amplitude of this oscillation is much smaller.

It should be noted that the structural and geometric conditions of the robot are similar in both cases. In Fig. 8, the step torque applied to the joints returns the robot to its original position in the water. When in the air, the first link rotates about 14° and the second link experiences a rotation of almost 42°. Thus, considering the effect of water compared to

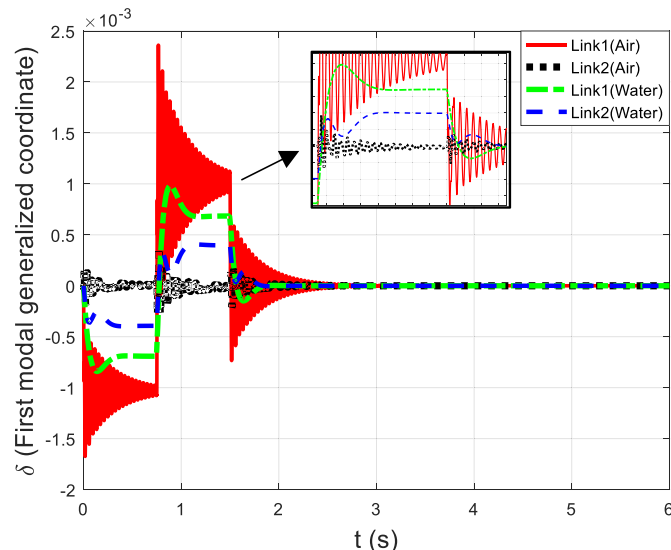


Fig. 9. Links first generalized modal coordinates.

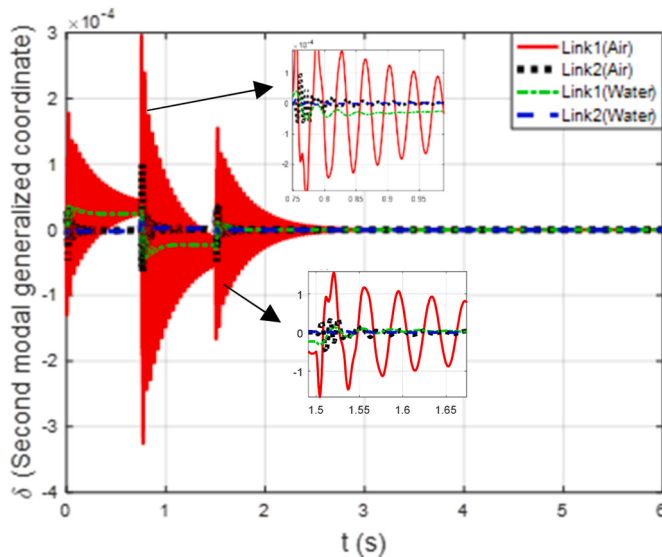


Fig. 10. Links second generalized modal coordinates.

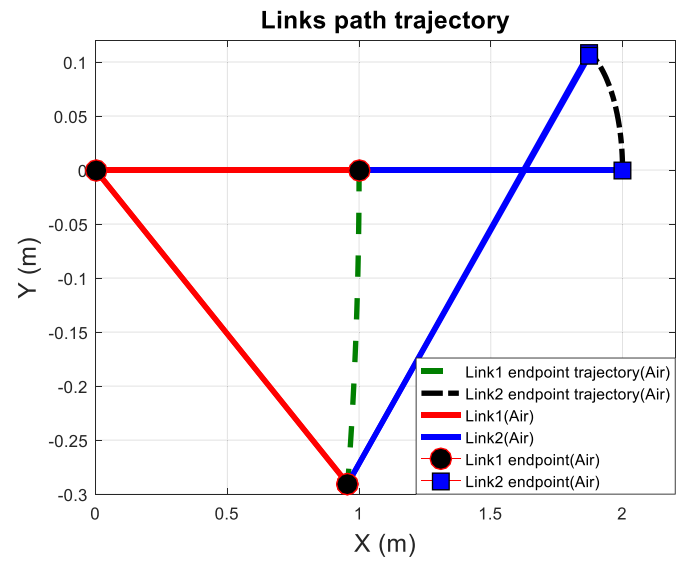


Fig. 12. Robot's path in air media.

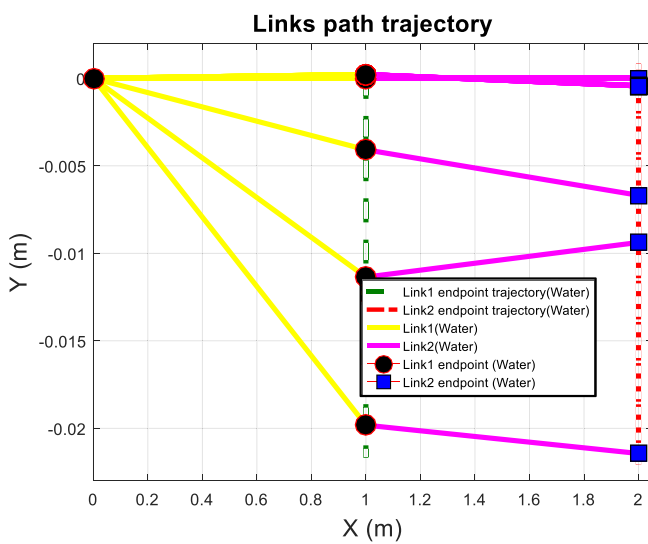


Fig. 11. Robot's path in water media.

the air corroborates the results, and the fluid-structure interaction stops the robot motion in the form of a resistive force, the effect of which cannot be ignored.

Figs. 9 and 10 show the first and second generalized modal coordinates based on which the elastic deformation of robot links is calculated. The results show that by changing the surrounding medium from air to water, the magnitude of the modal coordinates decreases by an average of 30%. However, the amplitude of oscillation and its frequency are adapted to the new environmental conditions, and as a result, the system oscillation frequency is reduced. The momentum caused by the torque applied to the robot joints in the direction of the link rotation is the reason behind the deviation from the neutral axis in both cases. The mentioned effect is more visible in the first mode than the second mode.

Figs. 11 and 12 show the robot trajectory in the air and water, respectively. This path includes the trajectory of the second link's joint and the robot gripper. According to Fig. 12, the gripper of the first link (the joint of the second link) is moved by 0.3 m in the air. In contrast, the robot gripper moves 0.23 m. By examining the robot's motion in the fluid, it is determined that the traveled path is 10% of the path in the air.

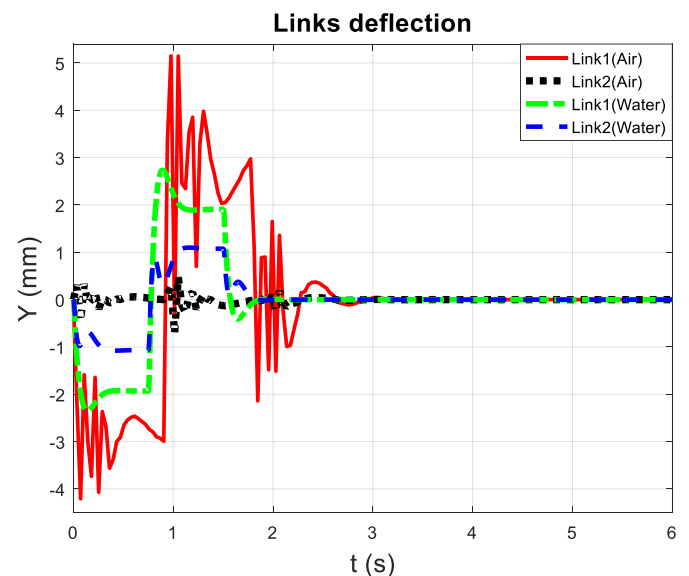
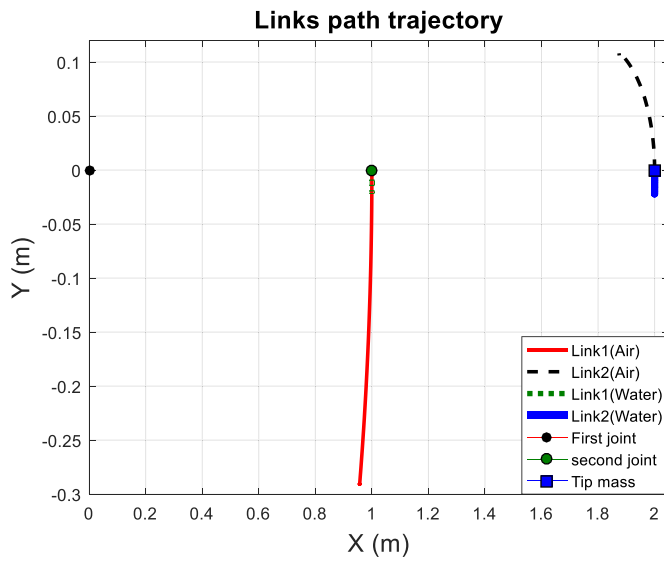


Fig. 13. The comparison of robot's links deflection in air and water media.

Also, this is a reciprocating trajectory in the water. This means that when a positive torque is applied, the robot moves forward and when a negative torque is applied, the robot acts in the opposite direction. On the other hand, when a negative torque is applied in the air, the velocity, not its direction, changes. This difference is due to the fluid environment in the two modes of motion.

Fig. 13 shows the elastic deformation of the robotic arm on the traversed path. These findings indicate that the oscillation amplitude of the link in the air is about twice that in the water. This was also predictable based on the data obtained from the generalized modal coordinates. Careful examination of the results reveals that the elastic deformation of the second link in the air is less than that in the water. This is attributed to arm-fluid interaction, which generates the elastic deformation of the link as it moves in the fluid. Fig. 14 shows the difference between the trajectories of the first and second arm's gripper in both air and water. The difference in the robot motion albeit with similar inputs is evident.



**Fig. 14.** The comparison of robot's path in air and water media.

**Table 3**  
Mechanical characteristic of the underwater flexible robotic chain.

Parameter	Description	Value
$E_1 = E_2$	Links Elasticity	$\text{case1} : 0.7 \times 10^9 \text{ N}\cdot\text{m}^{-2}$ , $\text{case2} : 0.7 \times 10^{10} \text{ N}\cdot\text{m}^{-2}$ , $\text{case3} : 0.7 \times 10^{11} \text{ N}\cdot\text{m}^{-2}$ , $\text{case4} : 0.7 \times 10^{12} \text{ N}\cdot\text{m}^{-2}$
$\gamma_w$	Water damping coefficient	$0.8 \frac{\text{Kg.s}}{\text{m}}$

#### 4.2. Simulation of underwater robot motion in view of links elasticity

In this section, by changing the elasticity of robot links, the effect of fluid-manipulator interaction is investigated. Table 3 shows the mechanical characteristics of the utilized flexible robotic chain. Other specifications of the robot are similar to Tables 1 and 2. The estimated time for the robot's motion is 6 s.

The robot starts moving from a position with the initial conditions  $\{\theta_1 = \theta_2 = \delta_{11} = \delta_{12} = \delta_{21} = \delta_{22} = 0\}$ . The simulation continues while the torque is applied to the joints of the first and second link as shown in

**Fig. 15.** In view of the interaction between the arms and the water, the motion is recorded after removing the motor torque until the robot stops.

In the following, the obtained response for the system motion is evaluated for different elasticities of robot links. Fig. 16 shows the changes in the angle of joints with respect to manipulator elasticity.

As the link elasticity increases, the motion amplitude of both joints decreases, Fig. 16, although the input torque and robot structure remain the same. One concludes that the effect of fluid-robot interaction increases if the link is harder (stiffer), preventing the robot from rotating. The step torque applied to the robot according to Fig. 15 acts similar to the rotational motion brake of the robot links, although the amount of movement of the second link is different from that of the first link while similar torques are applied to the joints of both links. This amount is much higher in the second link as no load is applied to the robot gripper. In the first arm, the interaction between the first and second links, and the effect of the motor of the second joint slows down the rotational motion of the robot.

Figs. 17 and 18 respectively show the first and second generalized modal coordinates. Similar to the discussion in Fig. 16, the fluid-manipulator interaction has increased the vibration amplitude of the robot. This amplitude is higher in the first link due to the impact of the second link. However, with the increasing stiffness of robot links, the amount of these oscillations decreases. In a way, with decreasing link elasticity and consequently decreasing the stiffness of robot links, the vibration modes experience growth and decline during motion. The fluid increases this amplitude due to its resistive effect and decreases its oscillation frequency.

Fig. 19 shows the trajectory of the robot gripper and its second joint. The path of the gripper of each link is also drawn separately. With the increasing flexibility of robot links and decreasing elasticity, the amplitude of motion and oscillation increases, although the system torque inputs are the same in all cases. Thus, the interaction between the fluid and robot links increases the oscillation amplitude and motion range of the robot.

Fig. 20 shows the deformation of robot links during motion. The obtained results confirm the accuracy of obtained equations based on the analyses presented for previous figures. It can be concluded that the links undergo deformation due to the effect of fluid force on the links during motion. This deformation increases with decreasing robot link strength. However, the way the torque is applied is also influential.

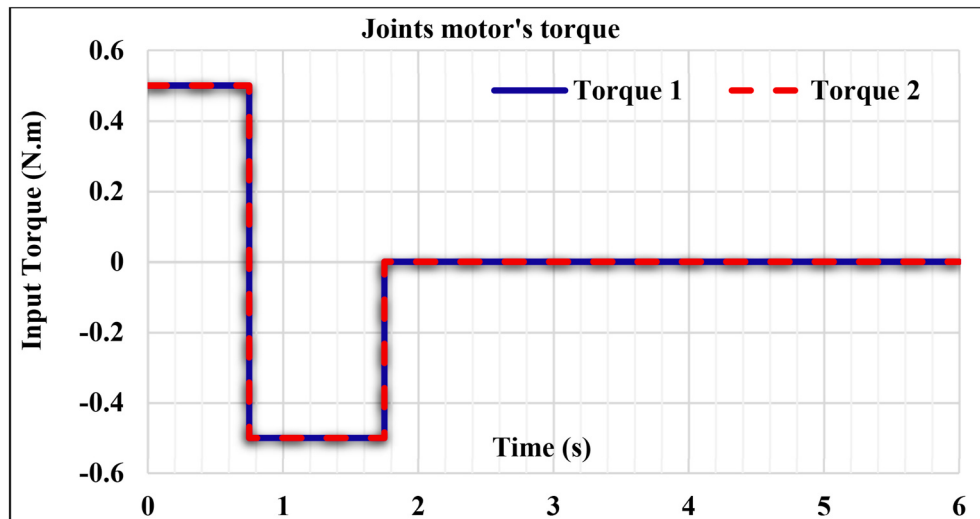


**Fig. 15.** Exerted torque to the joints of the two-link flexible robotic chain.

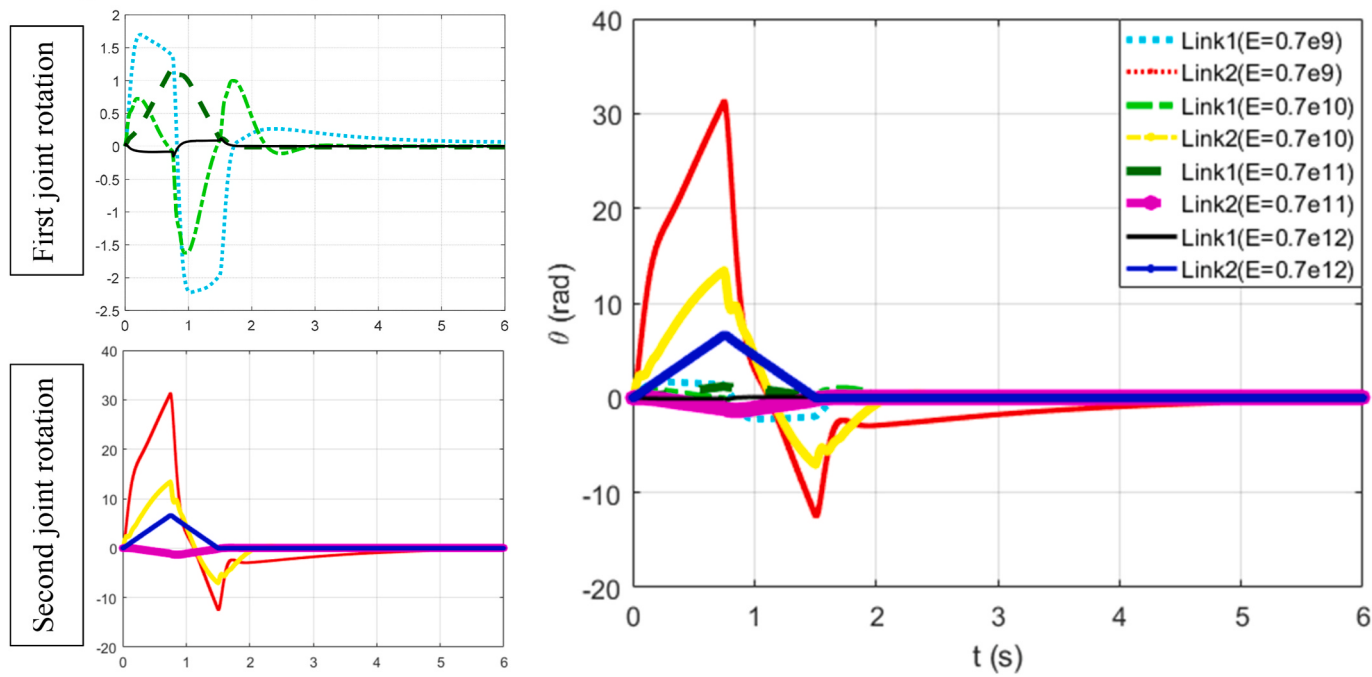


Fig. 16. Exerted torque to the joints of the two-link flexible robotic chain.

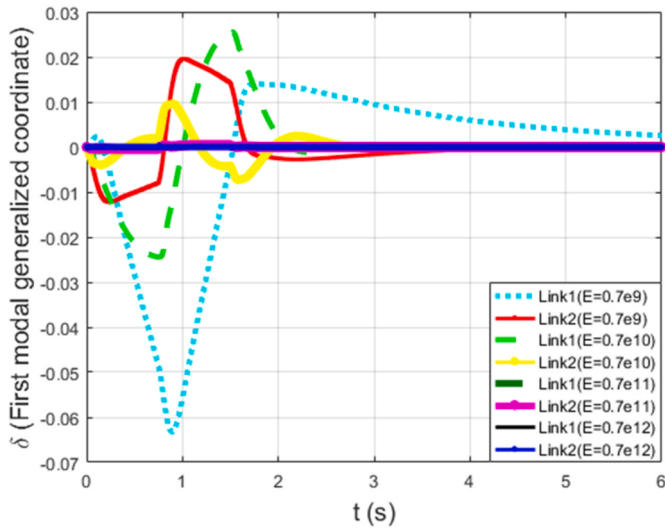


Fig. 17. Links first generalized modal coordinates.

#### 4.3. Simulation of underwater robot motion in view of initial conditions of motion

In this section, by changing the initial conditions of motion, the effect of fluid-manipulator interaction is investigated. Table 4 shows the mechanical specifications of the flexible robotic chain used in this section (other properties are reported in Tables 1 and 2).

The robot is considered to be on the ZX plane, starting its motion from rest in the fluid as a result of gravity with no torque being applied to its joints and continuing its motion until it fully stops.

Fig. 21 shows the elastic deformation of robot links along the robot path. The difference in the manipulator deformation indicates a difference at the time of release and the path traversed by the robot arms. According to the results, the time to reach the maximum deformation for both links is different in these two cases. Fig. 22 shows the robot trajectory for two different sets of initial conditions. One observes that

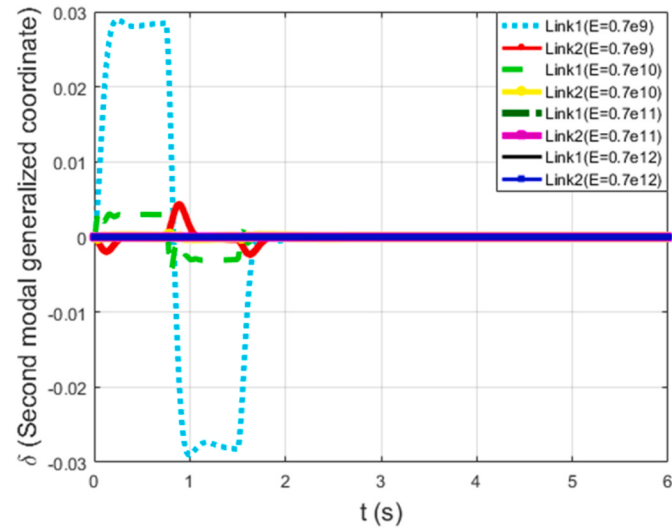


Fig. 18. Links second generalized modal coordinates.

different initial conditions result in different behaviors owing to the impact of the fluid-flexible arm interaction. Under similar conditions, this path is different from the path in the air as discussed in earlier studies. The path traveled by the robot gripper in water determines the effect of water-flexible arms. The displacement of the gripper of the flexible arm is 4 m in the first case and 3 m in the second case.

#### 5. Summary and conclusions

By developing the dynamic model of underwater flexible manipulators, the new equations of motion of the flexible robotic system are derived in this study. This necessitates examining the dynamic interaction between the fluid and the robot arms so that the amount of applied force and torque in the equations of motion can be identified. Next, the resulting hydrodynamic and hydrostatic effects are considered to obtain the final equations of motion. Compared to previous research, the use of

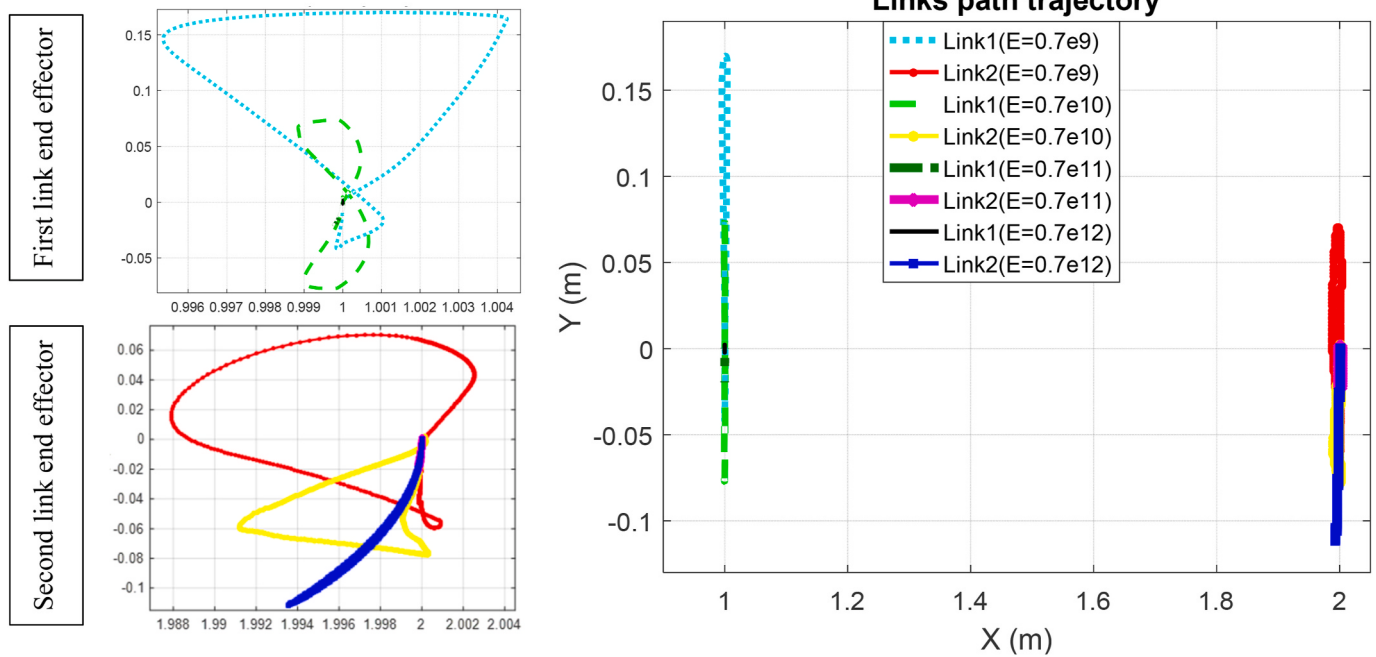


Fig. 19. Robot trajectory including the grippers of the first and second link.

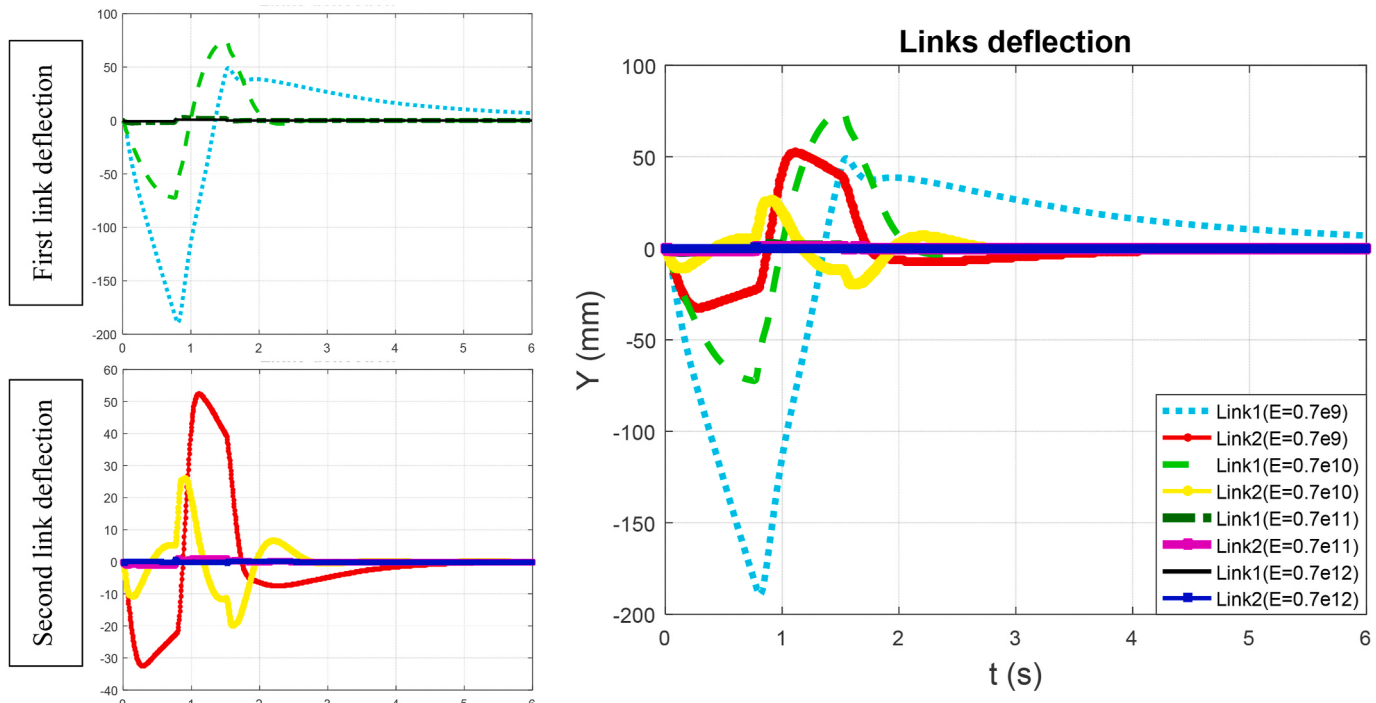
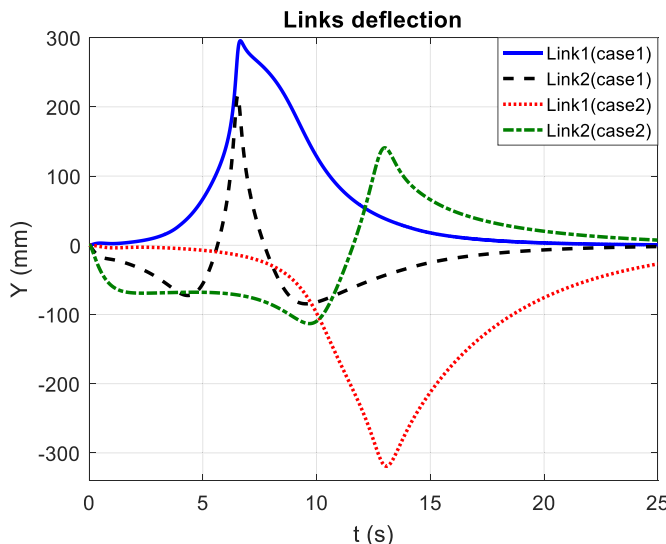


Fig. 20. Deformation of the first and second link.

**Table 4**  
Mechanical characteristics of the underwater flexible robotic chain.

Parameter	Description	Value
$E_1 = E_2$	Links Elasticity	$0.7 \times 10^{10} N \cdot m^{-2}$
$\{\theta_1, \theta_2, \delta_{11}, \delta_{12}, \delta_{21}, \delta_{22}\}$	Initial conditions	case1 : {90, 0, 0, 0, 0, 0} case2 : {90, -90, 0, 0, 0, 0}

flexible links allows us to calculate the impact of hydrostatic, hydrodynamic, and buoyancy interactions along the arm as a distributed function, hence improving the accuracy of final equations. The rigid-body motion of the robot affects the elastic deformation of manipulators. In addition, the fluid (specifically, its density) and the initial conditions for the robot's motion affect its path. The recursive Gibbs-Appell formulation is used to derive the dynamic equations. In view of the equations of force and torque due to the nature of the fluid which are nonlinear and complex, this type of formulation makes it possible to consider these restoring forces and torques when updating the general



**Fig. 21.** Flexible links deformation by considering different initial conditions.

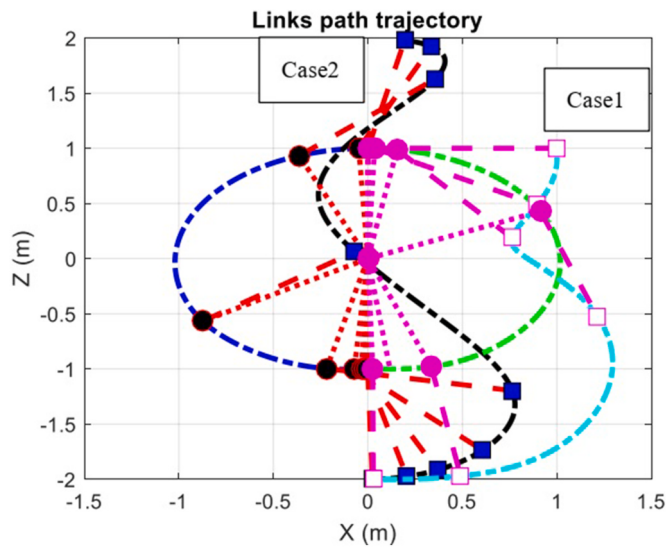


**Fig. 22.** Robot path with considering the different initial conditions.

Gibbs-Appell equations and use them in the Rayleigh dissipation function. This formulation also reduces the size of calculations as well as the complexity of deriving the final equations of motion compared to similar techniques. The equations of the N-link robotic chain can thus be obtained in a general form. Simulating the obtained equations of motion show that, compared to air, the deformation of flexible links decreases from about a maximum of 5 mm–3 mm, while the rigid-body motion of the system in the same direction decreases by 90% due to the fluid-arm interaction. Other comparisons are conducted for different values of link elasticity and initial conditions of the robot motion. It is observed that the link elasticity and the surrounding medium of the robot affect the deformation of manipulators and the oscillation frequency. Different initial conditions also confirm the effect of surrounding medium and hydrodynamic interactions in terms of the starting point. The final model of the underwater flexible robot can be used in controlling flexible chains to displace objects, inspect oil and power transmission lines, and explore oil resources.

## CRediT authorship contribution statement

**S.F. Dehkordi:** Conceptualization, Methodology, Software, Data curation, Writing – original draft, Visualization, Investigation, Validation.

## Declaration of competing interest

The authors declare that they have no known competing financial interests or personal relationships that could have appeared to influence the work reported in this paper.

## Appendix A. Supplementary data

Supplementary data to this article can be found online at <https://doi.org/10.1016/j.oceaneng.2021.110057>.

## References

- Al-khafaji Ali, A.M., Darus, I.Z.M., 2014. Finite element method for dynamic modelling of an underwater flexible single-link manipulator. *J. Vibroengineering* 16, 3620–3636.
- Antonelli, G., Fossen, T.I., Yoerger, D.R., 2008. Underwater robotics. In: Springer Handbook of Robotics. Springer Berlin Heidelberg, Berlin, Heidelberg, pp. 987–1008. [https://doi.org/10.1007/978-3-540-30301-5\\_44](https://doi.org/10.1007/978-3-540-30301-5_44).
- Cai, M., Wang, Y., Wang, S., Wang, R., Ren, Y., Tan, M., 2020. Grasping marine products with hybrid-driven underwater vehicle-manipulator system. *IEEE Trans. Autom. Sci. Eng.* 1–12 <https://doi.org/10.1109/TASE.2019.2957782>.
- Craig, John J., 2018. In: *Introduction to Robotics: Mechanics and Control*, fifth ed. Pearson.
- Goheen, K.R., 1991. Modeling methods for underwater robotic vehicle dynamics. *J. Rob. Syst.* 8, 295–317. <https://doi.org/10.1002/rob.4620080303>.
- Gümüşel, L., Özmen, N.G., 2011. Modelling and control of manipulators with flexible links working on land and underwater environments. *Robotica* 29, 461–470. <https://doi.org/10.1017/S0263574710000305>.
- Han, S.M., Benaroya, H., Wei, T., 1999. Dynamics OF transversely vibrating beams using four engineering theories. *J. Sound Vib.* 225, 935–988. <https://doi.org/10.1006/jsvi.1999.2257>.
- Huang, H., Tang, Q., Li, H., Liang, L., Li, W., Pang, Y., 2017. Vehicle-manipulator system dynamic modeling and control for underwater autonomous manipulation. *Multibody Syst. Dyn.* 41, 125–147. <https://doi.org/10.1007/s11044-016-9538-3>.
- Kabe, A.M., Sako, B.H., 2020. Damping. In: *Structural Dynamics Fundamentals and Advanced Applications*. Elsevier, pp. 173–219. <https://doi.org/10.1016/B978-0-12-821614-9.00004-5>.
- Kolodziejczyk, W., 2018. The method of determination of transient hydrodynamic coefficients for a single DOF underwater manipulator. *Ocean Eng.* 153, 122–131. <https://doi.org/10.1016/j.oceaneng.2018.01.090>.
- Korayem, M.H., Dehkordi, S.F., 2017. Derivation of dynamic equation of viscoelastic manipulator with revolute-prismatic joint using recursive Gibbs-Appell formulation. *Nonlinear Dynam.* 89, 2041–2064. <https://doi.org/10.1007/s11071-017-3569-z>.
- Korayem, M.H., Dehkordi, S.F., 2019. Motion equations of cooperative multi flexible mobile manipulator via recursive Gibbs-Appell formulation. *Appl. Math. Model.* 65 <https://doi.org/10.1016/j.apm.2018.08.035>.
- Korayem, M.H., Shafei, A.M., 2013. Application of recursive Gibbs-Appell formulation in deriving the equations of motion of N-viscoelastic robotic manipulators in 3D space using Timoshenko Beam Theory. *Acta Astronaut.* 83, 273–294. <https://doi.org/10.1016/j.actaastro.2012.10.026>.
- Korayem, M.H., Shafei, A.M., Dehkordi, S.F., 2014. Systematic modeling of a chain of N-flexible link manipulators connected by revolute-prismatic joints using recursive Gibbs-Appell formulation. *Arch. Appl. Mech.* 84, 187–206. <https://doi.org/10.1007/s00419-013-0793-y>.
- Korayem, M.H., Dehkordi, S.F., Mojarradi, M., Monfared, P., 2019. Analytical and experimental investigation of the dynamic behavior of a revolute-prismatic manipulator with N flexible links and hubs. *Int. J. Adv. Manuf. Technol.* <https://doi.org/10.1007/s00170-019-03421-x>.
- Korayem, M.H., Hedayat, A., Dehkordi, S.F., 2021. Dynamic modeling of cooperative manipulators with frictional contact at the end effectors. *Appl. Math. Model.* 90, 302–326. <https://doi.org/10.1016/j.apm.2020.08.078>.
- Lapierre, L., Fraisse, P., Dauchez, P., 2003. Position/force control of an underwater mobile manipulator. *J. Rob. Syst.* 20, 707–722. <https://doi.org/10.1002/rob.10119>.
- Lee, T.S., Alandoli, E.A., 2020. A critical review of modelling methods for flexible and rigid link manipulators. *J. Brazilian Soc. Mech. Sci. Eng.* 42, 508. <https://doi.org/10.1007/s40430-020-02602-0>.
- Lionel, L., 2006a. Underwater robots Part I: current systems and problem pose. In: *Mobile Robots: Towards New Applications*. I-Tech Education and Publishing. <https://doi.org/10.5772/4697>.
- Lionel, L., 2006b. Underwater robots Part II: existing solutions and open issues. In: *Mobile Robots: Towards New Applications*. I-Tech Education and Publishing. <https://doi.org/10.5772/4698>.

- Liu, Z., Liu, J., 2020. Dynamic modeling and vibration control for a nonlinear three-dimensional flexible manipulator. [https://doi.org/10.1007/978-981-15-2596-4\\_9](https://doi.org/10.1007/978-981-15-2596-4_9), 137–171.
- Mat Darus, I.Z., Al-Khafaji, A.A.M., 2021. Bio-inspired algorithms for modeling and control of underwater flexible single-link manipulator. [https://doi.org/10.1007/978-981-15-4917-5\\_35](https://doi.org/10.1007/978-981-15-4917-5_35), 483–496.
- McMillan, S., Orin, D.E., McGhee, R.B., 1995. Efficient dynamic simulation of an underwater vehicle with a robotic manipulator. *IEEE Trans. Syst. Man. Cybern.* 25, 1194–1206. <https://doi.org/10.1109/21.398681>.
- Mehrjooee, O., Fathollahi Dehkordi, S., Habibnejad Korayem, M., 2019. Dynamic modeling and extended bifurcation analysis of flexible-link manipulator. *Mech. Base. Des. Struct. Mach.* 1–24. <https://doi.org/10.1080/15397734.2019.1665542>.
- Minoo H Patel, n.d. Dynamics of Offshore Structures, 27th ed. Butterworth-Heinemann.
- Mohammed, M.J., 2018. A comparison study of underwater and land flexible manipulators. *Eng. Technol.* J. 36 <https://doi.org/10.30684/etj.36.6A.11>.
- Mohammed, M.J., Abbas, B.A., Al-Azawiey, S.A., 2019. Flexible underwater manipulator modelling using intelligent method. *Int. J. Mech. Eng. Robot. Res.* 860–866. <https://doi.org/10.18178/ijmerr.8.6.860-866>.
- Pettersen, K.Y., Fossen, T.I., 2018. Guidance of autonomous underwater vehicles. In: Encyclopedia of Robotics. Springer Berlin Heidelberg, Berlin, Heidelberg, pp. 1–10. [https://doi.org/10.1007/978-3-642-41610-1\\_11-1](https://doi.org/10.1007/978-3-642-41610-1_11-1).
- Qiu, Z., Li, C., Zhang, X., 2019. Experimental study on active vibration control for a kind of two-link flexible manipulator. *Mech. Syst. Signal Process.* 118, 623–644. <https://doi.org/10.1016/j.ymssp.2018.09.001>.
- Rong, B., Rui, X., Tao, L., Wang, G., 2019. Theoretical modeling and numerical solution methods for flexible multibody system dynamics. *Nonlinear Dynam.* 98, 1519–1553. <https://doi.org/10.1007/s11071-019-05191-3>.
- Salloom, T., Yu, X., He, W., Kaynak, O., 2020. Adaptive neural network control of underwater robotic manipulators tuned by a genetic algorithm. *J. Intell. Rob. Syst.* 97, 657–672. <https://doi.org/10.1007/s10846-019-01008-y>.
- Sharifnia, M., 2018. A new beam element for analysis of planar large deflection. *J. Brazilian Soc. Mech. Sci. Eng.* 40, 92. <https://doi.org/10.1007/s40430-018-0970-6>.
- Sharma, A.K., Saha, S.K., 2021. Simplified drag modeling for the dynamics of an underwater manipulator. *IEEE J. Ocean. Eng.* 46, 40–55. <https://doi.org/10.1109/JOE.2019.2948412>.
- Sharma, A.K., Abhishek, V., Saha, S.K., Srinivasa Reddy, N., Sen, S., 2019. Dynamic analysis of underwater vehicle-manipulator systems. [https://doi.org/10.1007/978-981-10-8597-0\\_63](https://doi.org/10.1007/978-981-10-8597-0_63), 739–748.
- Sivčev, S., Coleman, J., Omerdić, E., Dooly, G., Toal, D., 2018. Underwater manipulators: a review. *Ocean Eng.* 163, 431–450. <https://doi.org/10.1016/j.oceaneng.2018.06.018>.
- Tarn, T.J., Shoultz, G.A., Yang, S.P., 1996. A dynamic model of an underwater vehicle with a robotic manipulator using kane's method. In: Underwater Robots. Springer US, Boston, MA, pp. 195–209. [https://doi.org/10.1007/978-1-4613-1419-6\\_11](https://doi.org/10.1007/978-1-4613-1419-6_11).
- Underwater Robots, second ed., 2006. Springer Tracts in Advanced Robotics, Springer-Verlag, Berlin/Heidelberg. <https://doi.org/10.1007/11540199>.
- Wang, Z., Cui, W., 2021. For safe and compliant interaction: an outlook of soft underwater manipulators. *Proc. Inst. Mech. Eng. Part M J. Eng. Marit. Environ.* 235, 3–14. <https://doi.org/10.1177/1475090220950911>.
- Wang, Y., Chen, B., Wu, H., 2018. Practical continuous fractional-order nonsingular terminal sliding mode control of underwater hydraulic manipulators with valve deadband compensators. *Proc. Inst. Mech. Eng. Part M J. Eng. Marit. Environ.* 232, 459–469. <https://doi.org/10.1177/1475090217753900>.
- Yuguang, Z., Fan, Y., 2019. Dynamic modeling and adaptive fuzzy sliding mode control for multi-link underwater manipulators. *Ocean Eng.* 187, 106202. <https://doi.org/10.1016/j.oceaneng.2019.106202>.
- Yuh, J., 1990. Modeling and control of underwater robotic vehicles. *IEEE Trans. Syst. Man. Cybern.* 20, 1475–1483. <https://doi.org/10.1109/21.61218>.